12-2008

The Adaptability of Langmuir Probes to the Pico-Satellite Regime

Andrew Jay Auman
Utah State University

THE ADAPTABILITY OF LANGMUIR PROBES

TO THE PICO-SATELLITE REGIME

by

Andrew J. Auman

A thesis submitted in partial fulfillment
of the requirements for the degree

of

MASTER OF SCIENCE

in

Physics

Approved by:

Jan J. Sojka Major Professor	Don Thompson Committee Member
Edmund Spencer Committee Member	Byron R. Burnham, Dean of Graduate Studies

UTAH STATE UNIVERSITY
Logan, Utah

2008

ABSTRACT

The Adaptability of Langmuir Probes

to the Pico-Satellite Regime

by

Andrew J. Auman, Master of Science

Utah State University, 2008

Major Professor: Dr. Jan J. Sojka
Department: Physics

The purpose of this thesis is to investigate whether it is feasible to use Langmuir probes on pico-satellites flying in low Earth orbit over mid- to low-latitude geographic regions. Following chapters on the expected ionospheric conditions and an overview of Langmuir probe theory, a chapter addressing the difficulties involved with pico-satellite Langmuir probes is presented. Also, the necessary satellite-to-probe surface area requirements in order to achieve confidence in pico-satellite Langmuir probe data, for the orbital regions of interest to this thesis, are stated.

(56 pages)

ACKNOWLEDGMENTS

I would like to thank the members of my committee (Dr. Jan Sojka, Dr. Don Thompson, and Dr. Edmund Spencer) for the many hours they have spent in providing me with the guidance I needed and the revisions my thesis needed. Special thanks are due to Dr. Don Thompson, who was willing to work closely with me (often at the drop of a hat) in order to see this through and to provide me with an expert's view into Langmuir probe theory (both theoretical and practical).

I would also like to thank my family and friends for their prayers, support, and confidence. The amount of dedication I was required to give to this thesis in order to complete it in such a limited time meant that I was left without the time to provide for my own needs. Had it not been for the generosity of my family and friends–financial and otherwise–it would not have been feasible for me to have completed this thesis in the time that was available. To all of those who came to my defense, thank you. To my roommates at the Retrohouse, thanks for keeping me sane, down to Earth, and well fed. Additionally, I want to express my gratitude to Neil and Jenette Hamilton, for reasons known to them. And most importantly I want to thank my parents, Barney and Jackie Auman. From financial to moral support, it has been by their help and encouragement that I've not only completed this thesis but have become who I am today. I don't think they could ever possibly understand how much I look up to, and respect, both them and their guidance. I have the best parents in the world.

And as my parents taught me to give credit where it is due, it most certainly needs to be mentioned that the completion of this thesis–and corresponding degree–came by divine providence. I don't understand why I have been as favored by God as I have. He has, without fail, *always* been there for me: guiding me down the path He would have me take, making it known to me what He would have me do, preparing the way before me, and providing me with the means (often miraculously) whereby to accomplish the things He asks of me. I have never walked alone. And although the path has never been easy, when I

turn around and look back at where I have come from, the only things I can see are blessings without end. In gratitude for the countless truth and blessings He has already given to me, I look toward the future with only one desire: to follow Him.

And to Histh, I'm sorry that our relationship was so short lived and ended up coming to so quick an end. You will be missed.

Andrew Auman

CONTENTS

LIST OF TABLES

LIST OF FIGURES

CHAPTER 1
INTRODUCTION

Pico-satellites are defined to be satellites less than 1 kg in weight [1]. Due to their small size they can be much more difficult to engineer than larger satellites, as weight and size constriants can limit the pico-satellite's ability to collect and store power, to transmit telemetry, to determine or control the attitude or orbit, to perform science, and more. However, with the advancement of technology, pico-satellites are becoming more and more prevalent. This is because they offer several advantages over larger satellites. One of these advantages is cost. Pico-satellites can be manufactured at several orders of magnitude lesser cost than large satellites. This lower cost allows for the construction of multiple satellites instead of a single satellite, and for an improved testbed for new flight hardware (as the financial risk associated with failure is less).

It would be of benefit and interest to be able to use pico-satellites to measure electron and ion densities and temperatures in Earth's ionosphere. If this were possible, the low cost associated with the construction of pico-satellites would make it more financially feasible to build a constellation of pico-satellites to measure these ionospheric quantities. With a constellation of satellites flying in formation along an obit, it would be possible to differentiate between temporal and spacial variations in electron and ion densities and temperatures in the ionosphere.

The purpose of this thesis is to address whether plasma theory allows for the use of Langmuir probes (LP), an instrument used to measure electron and ion densities and temperatures in plasmas, with pico-satellites for mid- to low-latitude low Earth orbit (LEO) missions. In Chapter 2 the ionosphere is discussed and the extremum in electron and ion densities and temperatures under which pico-satellite-based Langmuir probes must function is determined. In Chapter 3 general Langmuir probe theory is discussed, providing information on how Langmuir probes are used to measure plasma characteristics. Chapter 4 discusses the difficulties and limitations associated with using Langmuir probes on

pico-satellites, as determined by the theory presented in Chapter 3. It also presents the situations and conditions for which pico-satellite-based Langmuir probes can be used. The thesis concludes with Chapter 5, which provides a summary of the findings.

CHAPTER 2
EARTH'S IONOSPHERE

Since, for this thesis, Langmuir probes are being used to measure atmospheric plasmas, an understanding of the Earth's atmospheric environment is essential. This understanding will help determine what conditions to expect and will lead to whether pico satellite Langmuir probes can effectively measure those conditions. Accordingly, an overview of the characteristics of the Earth's atmosphere are presented here.

2.1 Earth's Neutral Atmosphere

Typically, the regions of the Earth's atmosphere are characterized by aggregate properties exhibited by either the neutral or ionized species. Although the present discussion centers mainly on the plasma environment, both methods for defining the regions of the atmosphere are covered. This is done as the complete dynamics of the atmosphere are characterized not only by the individual behaviors of the separate neutral and ionized species dynamics, but also by the interactions between both the neutral and ionized species. Additionally, the vast majority of ions in the plasma regions of the atmosphere are of terrestrial origin.

In terms of neutral species the regions of the atmosphere are, for the most part, determined by the temperature profiles of those neutral species. These regions are, from lowest to highest altitude: troposphere, stratosphere, mesosphere, thermosphere and exosphere.

The troposphere ranges from 0 to 10km and is characterized by a decrease in temperature as altitude increases, until a minimum of approximately -50 C. The main constituents of the atmosphere here are N_2 (78%), O_2 (21%) and trace gases (with Argon being the highest in concentration) [2]. Here, heat being radiated from the surface of the Earth, over both land and water masses, is absorbed by the atmosphere. As the atmosphere absorbs this heat and expands, cells of convection currents are created. These convections cells create wind and are responsible for most of Earth's terrestrial weather. Disturbances due to this convection are also carried higher into the atmosphere through wave propagation [2]. Most

commercial aircraft fly at tropospheric altitudes.

At an altitude of about 10 km, the decrease in atmospheric temperature ceases. The altitude of the atmosphere at which the temperature reaches this local minimum is called the tropopause, a boundary layer between the troposphere and stratosphere. Above the tropopause the temperature begins to increase with increasing altitude through the stratosphere, a region covering from an altitude of about 10 km up to 45 km. Within the stratosphere lies the ozone layer, a region of diffuse O_3 molecules which absorb much of the UV radiation entering the Earth's atmosphere [2]. High altitude jets, such as the Concorde or SR-71 Blackbird, can fly at lower stratospheric altitudes.

The stratopause is located at an altitude of approximately 45 km and is defined to be the location where the atmospheric temperature reaches a local peak, usually around 0 C [2]. At this point the mesosphere begins. It is again characterized by a decrease in temperature of the atmosphere, down to a local minimum value. It is within the mesosphere that both gravity and planetary waves propagate and noctilucent clouds form. Sounding rockets typically fly at and above mesospheric altitudes, and Space Ship One attained upper mesopheric altitudes during its flights [3]. Also, it is within this region that meteors and re-entering satellites can burn up, the density of the atmosphere above this region being too low to produce pressure shocks sufficient enough for significant heating. This vaporization of meteors produces trace amounts of iron in the mesosphere.

Above the mesosphere lies the mesopause, occurring at an altitude of about 95 km. Typically, the temperature of the mesopause is around -100 C [2]. From here the thermosphere begins. In the thermosphere the temperature of the atmosphere increases with altitude to a maximum temperature, typically under 2,000 C (although its magnitude can vary depending on the amount of solar activity), and remains more or less constant thereafter as altitude increases. Also in the low thermosphere, typically occuring around 100 km, is the turbopause [2]. The turbopause is important because it is the point at which the heterogeneous mixing of the neutral species ends and where the atmosphere molecular diffusion begins to separate the neutral species according to their mass. This leads to a

changing, altitude-dependent, ratio of neutral atmospheric constituents, with the densities of heavier particles falling off more rapidly as alititude increases [2]. It is at lower thermospheric altitudes that the aurora form and atmospheric tides manifest. Atmospheric tides can have a large effect on LEO and PEO spacecraft as these orbit altitudes lie within the thermosphere [4]. The orbits of space shuttles and the International Space Station lie in the lower thermosphere.

The thermosphere continues until the thermopause, also known as the exobase, at an altitude of about 500 km. As the temperature of the atmosphere remains constant at about 1,000 K throughout this altitude [5], the transition from thermosphere to thermopause/exobase to exosphere is not actually determined by temperature but by fluid characteristics. Namely, at and above the altitude of the exobase, the densities of the neutral species in the atmosphere are too low for those species to be treated as a fluid. This transition from fluid dynamics to individual neutral particle ballistics is what separates the thermosphere from the exosphere [2]. The exosphere continues in altitude so far as neutral species particles are found, extending beyond 1,000 km.

2.2 Profile of the Ionosphere

The ionosphere is the region of the Earth's atmosphere where both charged and neutral particle species exist; below the ionosphere the atmosphere is comprised solely of neutral particle species while the region above the ionosphere, the plasmasphere, is comprised almost entirely of charged particle species. Although extraterrestrial ions do exist in the ionosphere, the vast majority of the electrons and ions that make up Earth's ionosphere come from the ionization of terrestrial molecules by solar radiation (UV, EUV, X-ray, and corpuscular [4] [6]). On average, the ionosphere ranges in altitude from 60 km to 1,000 km [4]. The ionosphere is divided into several regions. Ranging from lowest to highest altitude these regions are: D, E, F_1, F_2, although the F_1 and F_2 regions combine into what is known as the F region in the night-side ionosphere. Unlike the neutral atmosphere where regions are categorized by the temperature of the species present, the regions of the ionosphere are

categorized by electron density and composition. This is possible due to the fact that, although there can be great variations in the magnitude of electron density, the basic shape of the ionosphere is retained under different geographic, temporal, and solar conditions. This basic shape takes on two forms: one for the nighttime ionosphere and one for the daytime ionosphere. FIG. 2.1 shows the diurnal variations in the electron density of the ionosphere over Logan, Utah on 22 September 1979, demonstrating these two basic ionospheric profiles. The regions of the ionosphere are also labeled on FIG. 2.1. It is of particular interest to note the difference in electron density between the daytime and nighttime ionosphere, where the nighttime ionosphere can be up to a couple of orders of magnitude lower in density than the daytime ionosphere. FIG. 2.1, as well as all subsequent data presented hereafter for electron and ion densities and temperatures, has been produced by modeling the ionosphere using the 2007 code base of the International Reference Ionosphere, or IRI. The IRI is an "empirical standard model of the ionosphere, based on all available data sources" developed and maintained by an international committee "sponsored by the Committee on Space Research (COSPAR) and the International Union of Radio Science (URSI)" [7]. It is currently the standard model for measuring ionospheric plasma densities and temperatures.

The regions of the ionosphere have been labeled in FIG. 2.1 for both the nighttime and daytime profiles. The lowest region of the ionosphere is the D region. The D region begins approximately at 60 km and typically ranges to 100 km. In this region of the ionosphere the plasma is weakly ionized and chemical processes drive the dynamics [2]. Also, the free electrons due to the ionizing effect of the UV, EUV, and X-ray radiation tend to attenuate radio waves in this region during daytime [8]. Various molecular ions, such as O_2^+, NO^+, and water cluster ions, can be found in the D region as shown by FIG. 2.2, which shows various ion densities as a function of altitude over Logan, Utah on 22 September 1979 LT 15:00 (as modeled by the IRI).

Above the D region, and extending to about 150 km is the E region. This region is sometimes also referred to as the Kennelly-Heaviside layer or just the Heaviside layer [8]. Like the D region, the E region contains weakly ionized plasma and is driven mainly by

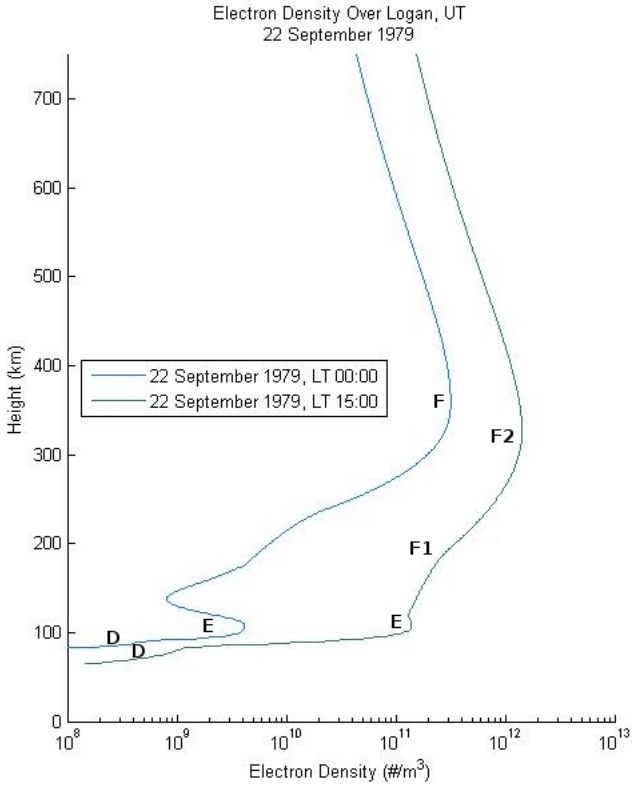

FIG. 2.1 Diurnal variations in electron density in the ionosphere.

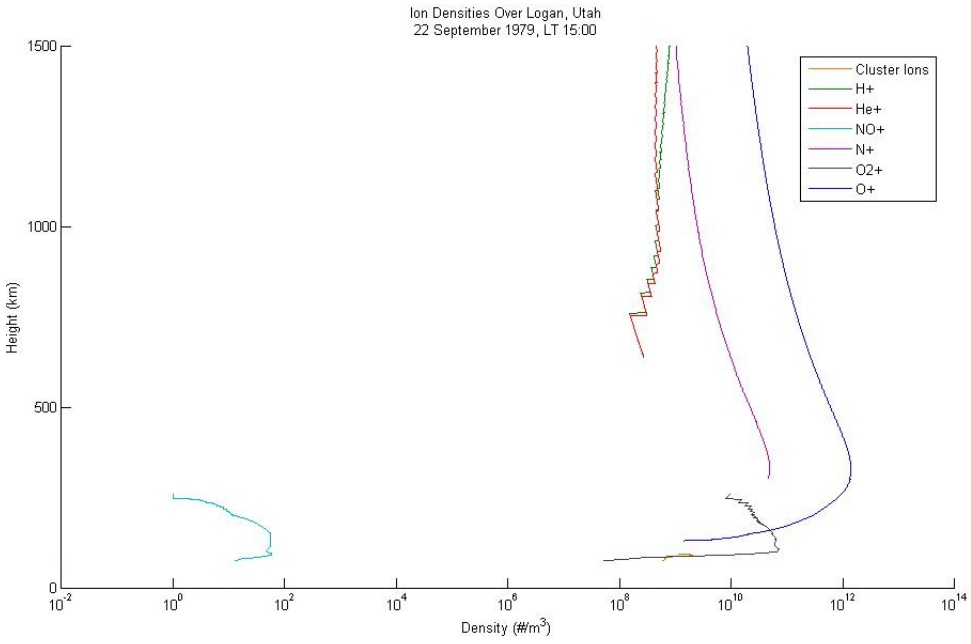

FIG. 2.2 Ion densities in the ionosphere during daytime at solar maximum.

chemical processes [2]. Accordingly, recombination diminishes the electron density on the night-side ionosphere allowing for increased radio wave propagation (as the height of the plasma layer off which radio waves are reflected is increased). The dominant ions responsible for this electromagnetic absorption and reflection are O_2^+ and NO^+. The dominant neutral particle species in both the D and E regions are N_2, O_2, and O [6].

The F region begins at 150 km and extends to the plasmasphere, at about 1,000 km [4] (although this height is greatly influenced by solar activity). On the day-side ionosphere, the F region separates into the F_1 (150 km to 250 km) and F_2 (250 km to 1,000 km) regions [4]. The F region contains the highest amounts of ionized particles, being principally dominated by O^+ ions (and with O as the dominant neutral species [6]). At this level of greatest ionization density in the Earth's atmosphere, called the F_2 peak (note that the night-side F peak is also simply referred to as the F_2 peak), electron densities can be greater than $10^6/\text{cm}^3$ during times of solar maximum. This peak density of greatest ionization is referred to as N_mF_2, and results from a large density gradient—as a function of altitude—in the neutral atmosphere in which incoming solar UV/EUV is absorbed, and is a complex balance between this ionization process, chemical recombination processes, and transport processes (such as ambipolar diffusion) [2]. The plasma frequency, defined as [2]

$$\omega_{p_j} = \left(\frac{n_j e^2}{\epsilon_0 m_j} \right)^{1/2}, \tag{2.1}$$

is the frequency at which electromagnetic waves are absorbed by plasma. For the F_1 region, this plasma frequency occurs at about 10 MHz. Accordingly, electromagnetic waves lower than this frequency are reflected off the F_1 region, while higher frequency electromagnetic radiation can pass through [8]. Further, according to [8], "The F_2 layer is the principal reflecting layer for HF communications during both day and night." Table 2.1 shows the plasma frequencies for the D, E, and F regions of the ionosphere over Logan, Utah on the given dates, as modeled by the 2007 IRI.

Above the F_2 peak, plasma transport processes begin to dominate ionospheric dynamics as altitude increases. This region, extending from the F_2 peak to the plasmasphere, is

TABLE 2.1 Plasma frequency, in MHz, for various regions during solar maximum and minimum.

	22 Sept 1979		22 Sept 1996	
	Night	Day	Night	Day
F	5.065	10.721	2.502	4.731
E	0.574	3.361	0.369	2.762
D	0.180	0.293	0.180	0.180

known as the topside ionosphere. Within the topside ionosphere the lighter H^+ and He^+ ions dominate [2]. Due to the large concentration of H^+ ions, this region is known as the protonosphere. Typically, the altitude at which the protonosphere begins is around 750 km, but depending on solar conditions can range anywhere from 500 km to 3,000 km [5]. In this region the plasma can be treated as being effectively fully ionized and collisions with neutral particles can be ignored [2].

2.2.1 Geographic Variations in the Ionosphere

As previously mentioned, although the basic daytime and nighttime profiles of the ionosphere are preserved for different geographical locations, the magnitudes of the electron and ion densities do change. There are three main geographic regions of interest: mid-, low-, and high-latitudes.

Mid-Latitude Regions

Of the three geographic regions in discussion, the mid-latitude regions of the ionosphere are the most simple. It is for this reason that this region is discussed first. Here, the ionospheric plasma corotates with the Earth [2] due to the influence of Earth's magnetic field, as given by Ferraro's Theorem [5]:

> In an equilibrium situation the angular velocity of the highly conducting plasma enclosed by the magnetic dipole field of a body rotating around the magnetic axis will be constant along the magnetic field lines, and the plasma is corotating with the body.

This corotation of plasma with the Earth occurs out to 6-7 R_e [5].

The only appreciable interaction of the plasma in these latitudes with the Earth's magnetic field is the possible trapping of electrons, due to their light mass, on magnetic field lines. Wind can then push these electrons along the magnetic field lines and into the conjugate ionosphere [2]. As stated in [2], since these dipole magnetic field lines vary in altitude with latitude, this can lead to topside ionosphere plasma transport to higher altitudes.

Low-Latitude Regions

In the low-latitude geographic regions of the ionosphere, Earth's magnetic field lines lie nearly perpendicular to the ground. This gives rise to an interesting dynamical process, known as the equatorial fountain [2]. Here, in the Earth's equatorial region, the wind blows in an eastward direction. Since the atmosphere in the low ionosphere is only weakly ionized, neutral particle-ion interactions are important. Accordingly, the eastward neutral wind carries the ionospheric plasma with it. This creates an electric field and, due to an $E \times B$ interaction with Earth's magnetic field, exhibits an upward force on the ionospheric plasma. This plasma then diffuses outward along the Earth's magnetic field lines, on both sides of the equator, while being pulled back down to lower altitudes by gravity. The end result of this process is an increased plasma density at the F_2 peak region of the day-side ionosphere within about 20 ° of both sides of the equator [5]. These regions of increased plasma density due to the equatorial fountain are known as the Appleton anomaly. A combination of both the equatorial fountain and the direct incident solar radiation also give rise to an increased F_2 peak height along the day-side equator.

The following figures show the effect of the equatorial fountain and subsequent Appleton anomaly. FIG. 2.3 shows both the F_2 peak density, N_mF_2 and height H_mF_2 along 180 ° longitude, graphed against latitude. In the top part of the graph the increased F_2 peak density bilateral to the equator is readily noticeable. The lower part of the graph shows that, even though the greatest F_2 peak densities occur at about 15 ° latitude, the maximum in F_2 peak height still occurs along the equator. Whereas FIG. 2.3 shows N_mF_2 for a slice

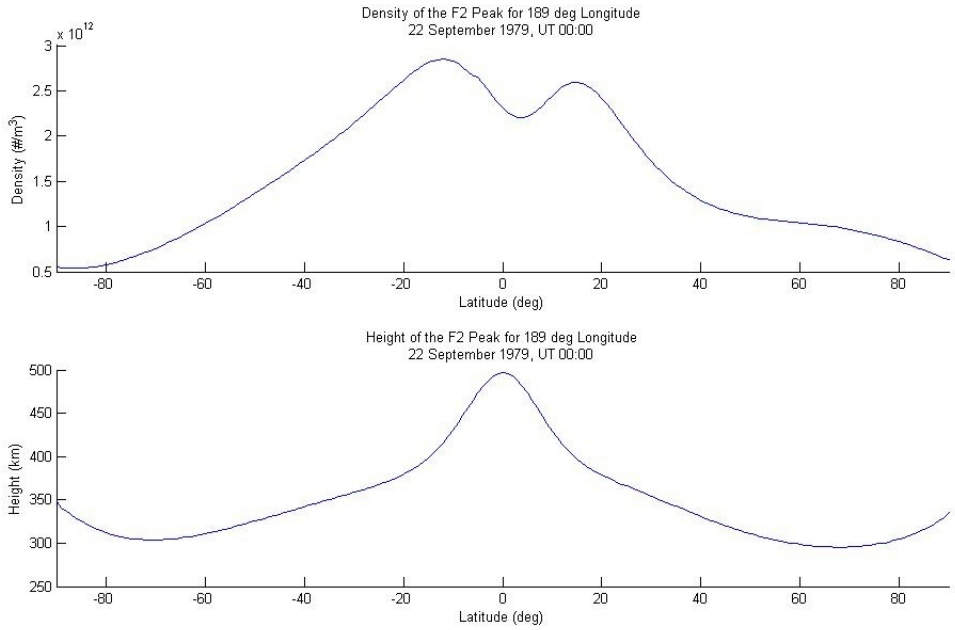

FIG. 2.3 F_2 peak densities and height for 189 ° longitude on 22 September 1979, Utah 00:00.

of the profile along one longitude, Figs. 2.4 through 2.7 show this profile on a global scale.

Another important low-latitude feature are equatorial bubbles. These plasma-depleted regions of the ionosphere can be up to hundreds of kilometers in length, and "can be up to two orders of magnitude lower than the surrounding medium" [2]. They are formed when a combination of $E \times B$ drift, neutral wind, and low-altitude night-side recombination sets up a Raleigh-Taylor instability. When this instability is perturbed by neutral wind or gravity waves, a density irregularity is created which allows for the lower-density, lower-altitude field-aligned areas of plasma depletions to form bubbles which propagate vertically at a rate of up to 500 m/s "while drifting with the background plasma" [2]. The plasma irregularities and inhomogeneities pre-cursing the formation of equatorial bubbles is known as spread F [2].

High-Latitude Regions

As stated by [6], in high-latitude regions the ionosphere is "strongly coupled to the solar wind-magnetosphere system via electric fields, auroral particle precipitation, electric

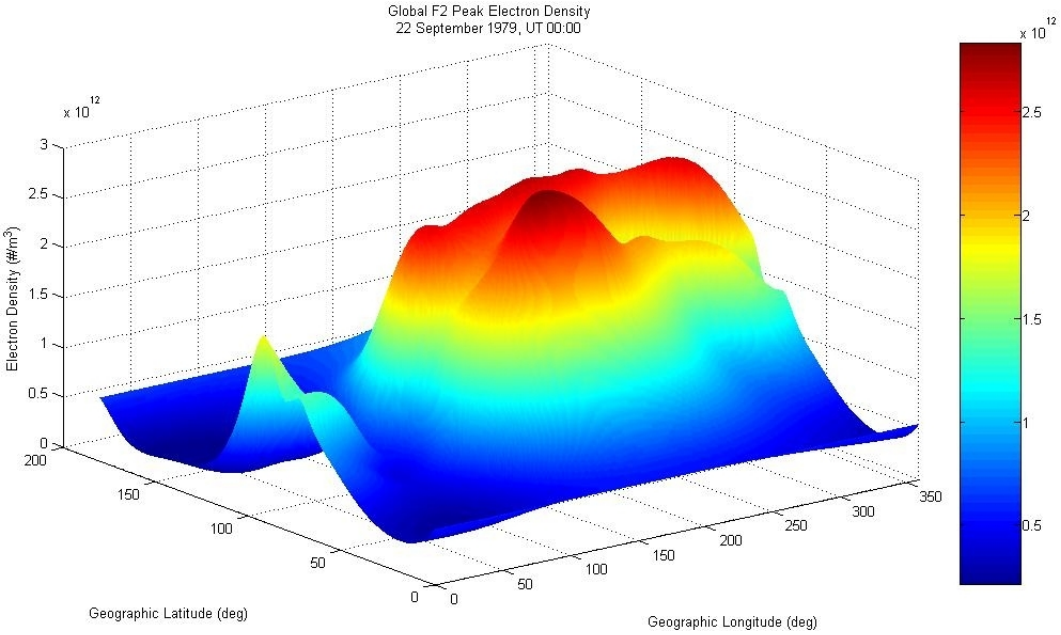

FIG. 2.4 Global F_2 peak electron density for 22 September 1979, Utah 00:00.

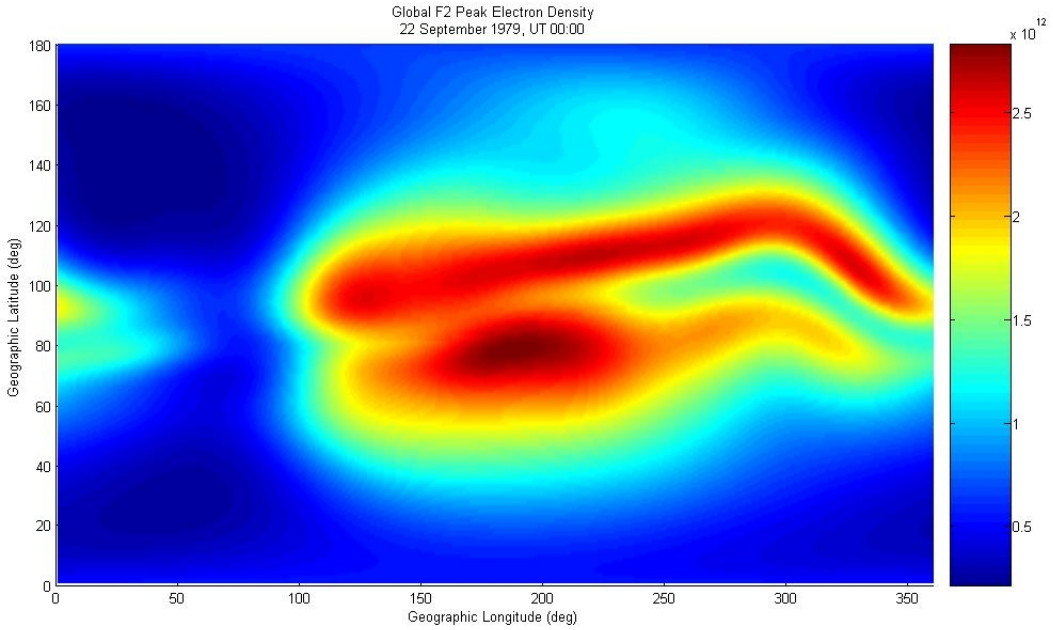

FIG. 2.5 Global F_2 peak electron density for 22 September 1979, Utah 00:00.

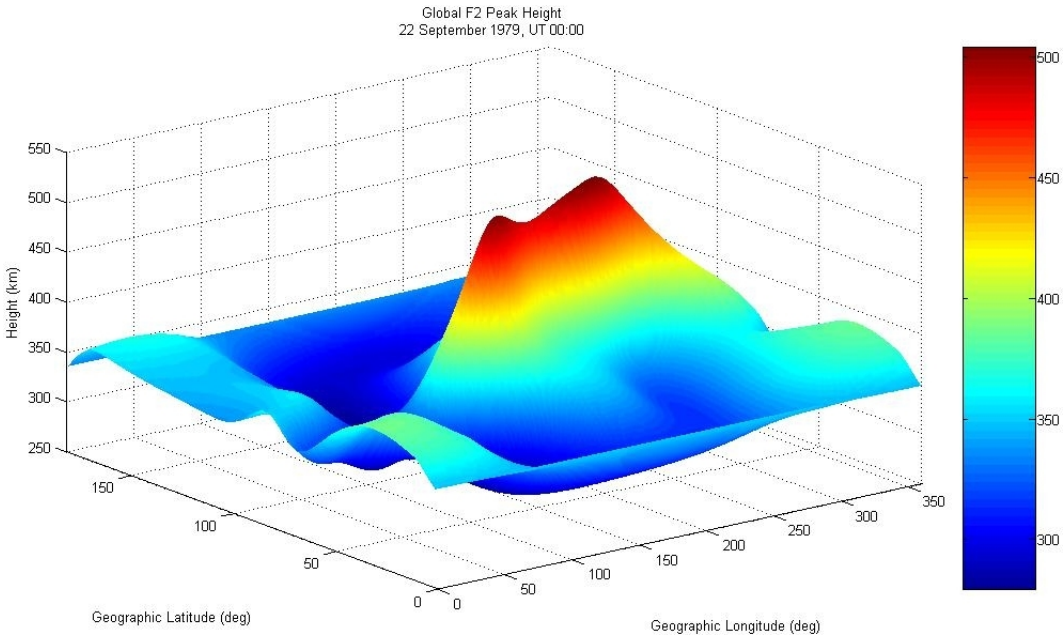

FIG. 2.6 Global F_2 peak height for 22 September 1979, Utah 00:00.

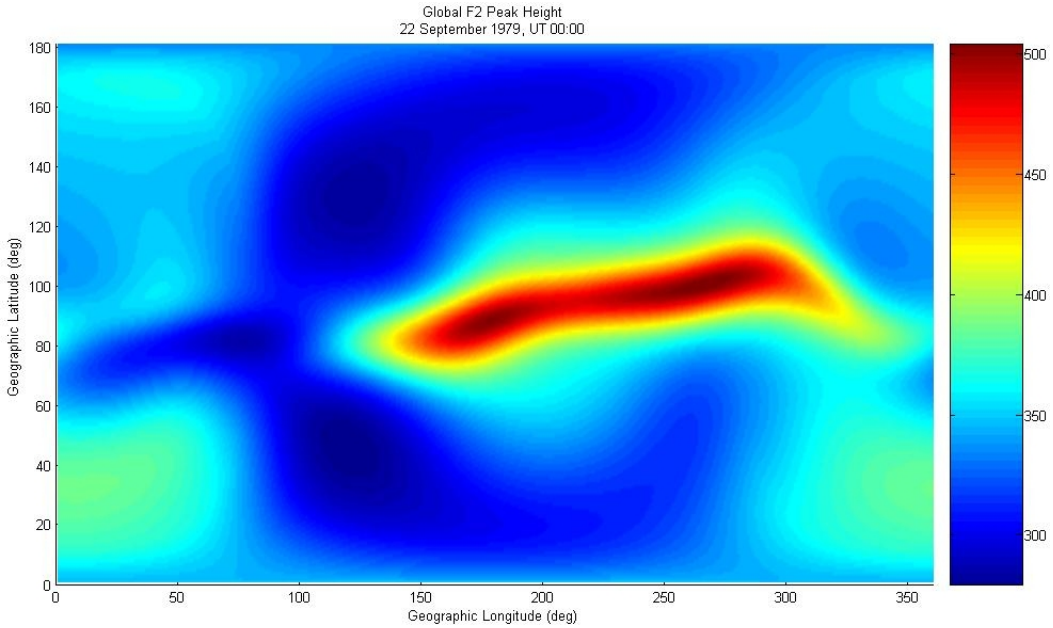

FIG. 2.7 Global F_2 peak height for 22 September 1979, Utah 00:00.

currents, and heat flows." Additionally, in these regions the Earth's magnetic field can be perpendicular, or nearly perpendicular, to the surface of the Earth. Because of these things, the high-latitude polar regions of the ionosphere are the most dynamic.

One of the high latitude anomalies arising from these complex high-latitude dynamics is a two-cell plasma flow pattern which develops in the polar regions. In the magnetosphere, due to the interaction of the solar wind with open magnetic field lines, electric potentials are created between magnetic field lines. These potentials are mapped down the magnetic field lines into the ionosphere and result in a dawn to dusk electric field across Earth's polar regions. Because of this electric field, plasma is drawn from the day-side ionosphere, across the poles, and into the night-side ionosphere [5]. This plasma diverges on the night-side ionosphere and continues to flow back to the day-side ionosphere at lower latitudes resulting in the two-cell flow pattern. However, it's important to note that this model is rather simplified and, as a result from more complex magnetospheric-ionospheric coupling, more complex multi-cell plasma flows typically develop [5].

Due to the fact that the electric fields in the high-latitude regions of the ionosphere lie perpendicular to the Earth's magnetic fields, auroral particles can move up and down the geomagnetic field lines with very little resistance [6]. As a result, the internal pressure of the ionospheric plasma pushes some of the topside ions upward into the magnetosphere. This outflow of topside ions is termed polar wind. This second anomaly can have a large effect on the density of the high-latitude ionosphere, especially in the F_2 peak region and topside ionosphere.

The most complex high-latitude region is the auroral oval. The auroral oval is an area of the Earth's atmosphere where highly energetic solar wind particles become trapped on Earth's magnetic field lines and are transported along those lines deep into the ionosphere. The auroral oval is shaped like a ring, centered about 3° toward midnight from the poles of Earth's magnetic field [4]. It is thinner in the day-side ionosphere than it is in the night-side ionosphere, where it can be up to 7° thick [9]. On the day-side ionosphere it typically extends down to 78° geomagnetic latitude, while on the night-side ionosphere it can get as

low as 67° geomagnetic latitude [5]—giving a 25° to 50° range in diameter under normal conditions. This auroral oval is in a state of constant flux due to solar wind energy and pressure, as well as magnetospheric-ionospheric coupling. Among these things, it is greatly influenced in its intensity by the dawn-dusk electric field which also causes the previously discussed two-cell plasma flow patterns. Auroral electron energies typically range from 2–21 keV while auroral ions typically range from 1–4 keV. However, electron temperatures could be greater than 40 keV, with ion temperatures greater than 20 keV, for auroral precipitation events during storm conditions [5].

2.2.2 Temporal Variations in the Ionosphere

As with geographic variations in the ionosphere, temporal ionospheric variations can be quite pronounced. There are three temporal periods of interest: diurnal, seasonal, and solar cycle.

Diurnal Variation

As the majority of plasma in the ionosphere is created by the ionization of terrestrial neutral particle species by solar UV, EUV and X-ray radiation, there is a dramatic difference between the day-side and night-side ionosphere plasma densities and temperatures. As previously discussed, the day-side ionosphere is divided into distinct regions: D, E, F_1, and F_2. As the solar UV, EUV, and X-ray radiation disappear at night, chemical processes drive the recombination of ions and electrons back into neutral species. This recombination is especially pronounced at lower altitudes where the density of the neutral atmosphere is greater. Due to this recombination, the ionospheric plasma densities decrease significantly at night resulting in the disappearance of the F_1 region and the near disappearance of the D region.

Within the F_2 region lies the F_2 peak, the area of greatest density of electrons and ions within Earth's atmosphere. Due to this high plasma density, the F_2 peak is often used as a proxy for characterizing the ionosphere as a whole. On a global scale, the greatest F_2 peak densities occur between 13:00 and 15:00 LT, due to the Earth's rotation. At night,

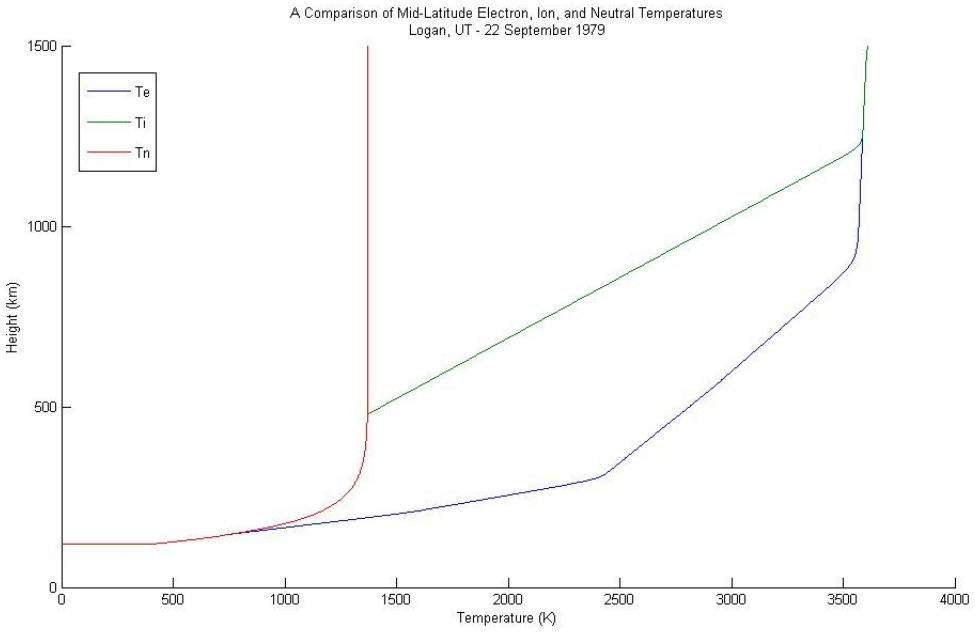

FIG. 2.8 A comparison of mid-latitude, daytime electron, ion, and neutral temperatures.

the F_2 peak density can drop by more than a factor of 10. The height of the F_2 peak also undergoes diurnal variations, with the night-side peak height occurring at greater altitudes. This is due to the loss of plasma at lower altitudes through chemical recombination and the lack of plasma production with the absence of solar radiation.

The temperature of the electrons, ions, and neutrals in atmosphere also varies throughout the day, with the highest temperatures occurring on the day-side ionosphere. The most important note here is that in general, as noted by [4], "[t]he electron temperature tends to be a factor of two greater than that of the neutrals, with the ion temperature falling in between." FIG. 2.8 shows typical mid-latitude electron, ion, and neutral daytime temperatures as modeled by the IRI.

FIG. 2.9 shows how the F_2 peak height and density change as a function of time over a given 24-hour period. Situated at mid-latitude, Logan, Utah was used for the model with 22 September 1979 as the date. Notice how the top graph shows th F_2 peak height occurring at 02:39 LT while the bottom graph shows the peak density occurring at 13:06 LT. FIG. 2.10

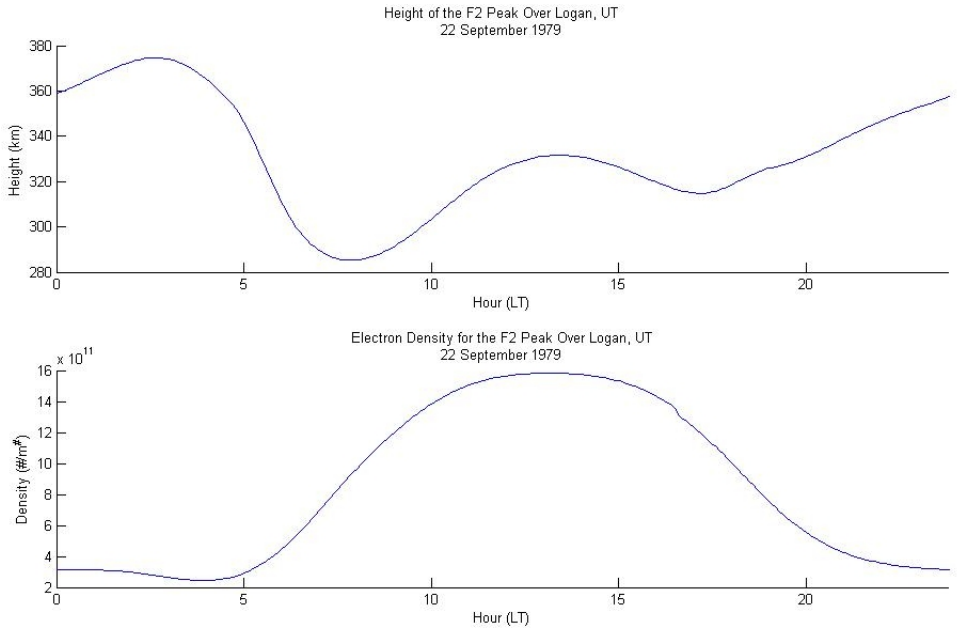

FIG. 2.9 Diurnal variation of the F2 peak height and density over Logan, Utah for 22 September, 1979.

shows the electron density as a function of altitude over Logan, Utah for various times on the same date.

Seasonal Variation

The seasonal variations in the ionosphere are a result in the changing solar zenith angle [2]. One would be led to believe that the electron density at the F_2 peak during summer months would be higher than it is in the winter months due to the smaller solar zenith angle in the winter [2]. However, due to strong coupling between the ionosphere and the thermosphere this is not the case. In fact, there is a markedly higher plasma density during the winter months than there is during the summer months, as shown by Figs. 2.11-2.12 which give nighttime and daytime mid-latitude N_mF_2 during winter and summer seasons (as modeled by the IRI). As [2] explains, "[T]he summer-to-winter neutral circulation results in an increase in the O/N_2 ratio in the winter hemisphere and a decrease in the summer hemisphere." It turns out that the production of plasma due to this increased density in neutral atomic oxygen far outweighs the plasma production due to increased solar radiation,

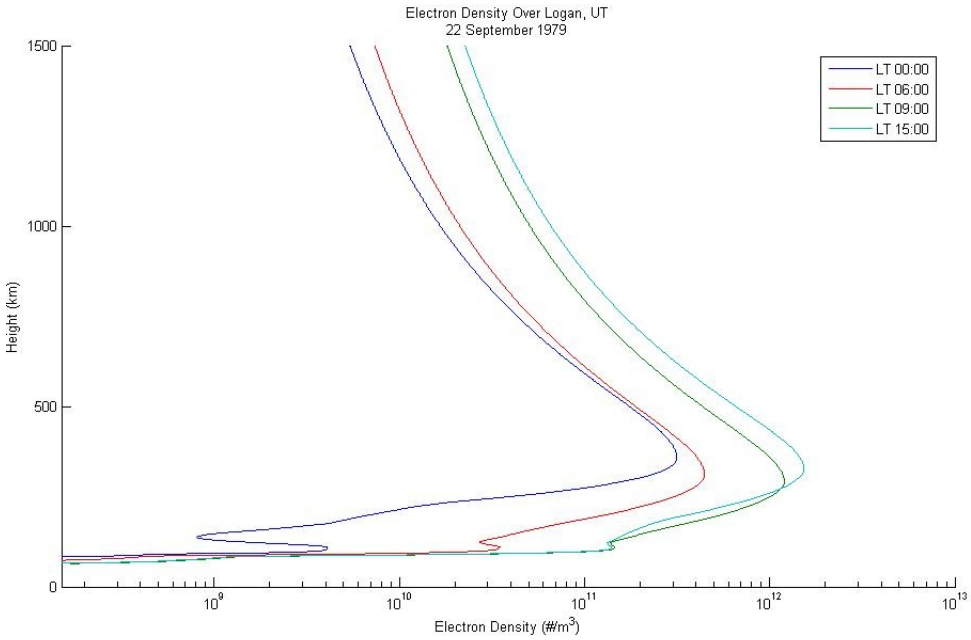

FIG. 2.10 Electron density profiles for various times of day over Logan, Utah for 22 September, 1979.

and the result is an overall increase in F_2 peak density during the winter months [2]. This increased electron density, however, leads to lower electron temperature during the winter months [2].

Solar Variation

The intensity of the solar radiation varies cyclically with a period averaging 11.1 years [5]. This variation is termed the solar cycle and is related to the sunspot number. FIG. 2.13 shows the International Sunspot number from the year 1749 to present. This number is calculated by

$$R_i = k\,(10g + f)\,, \tag{2.2}$$

where g is the number of sunspot groups, f is the number of sunspots, and k is a normalization constant to account for variability for different observation points [5].

Insofar as a connection existing between solar radiation and sunspot number, there does exist a correlation between sunspot number and the large-scale structure of both the X-ray and 10.7 cm flux [5]. As solar radiation produces the majority of plasma in the ionosphere,

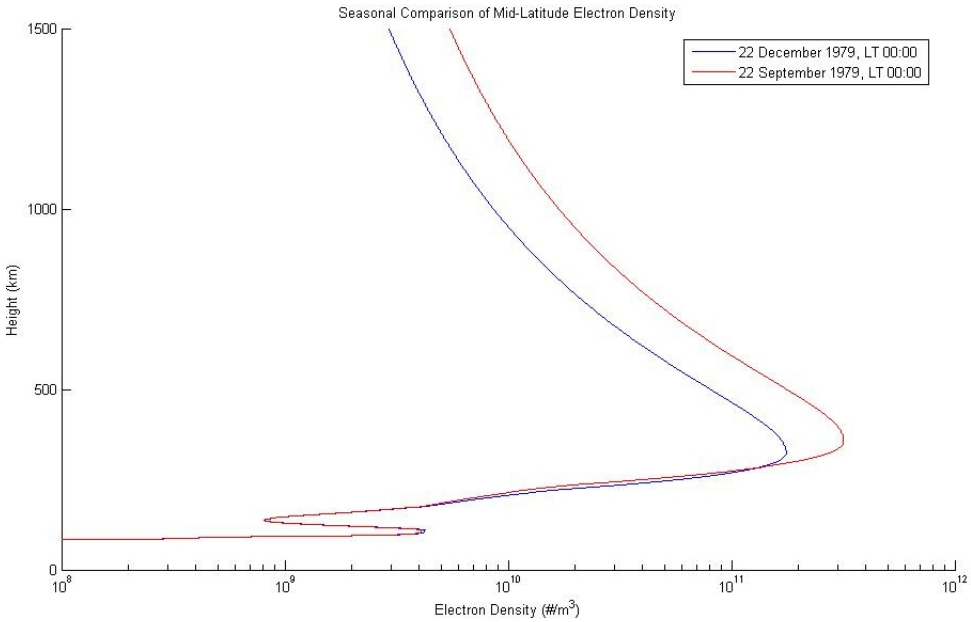

FIG. 2.11 Nighttime seasonal variation of electron density for mid-latitude regions.

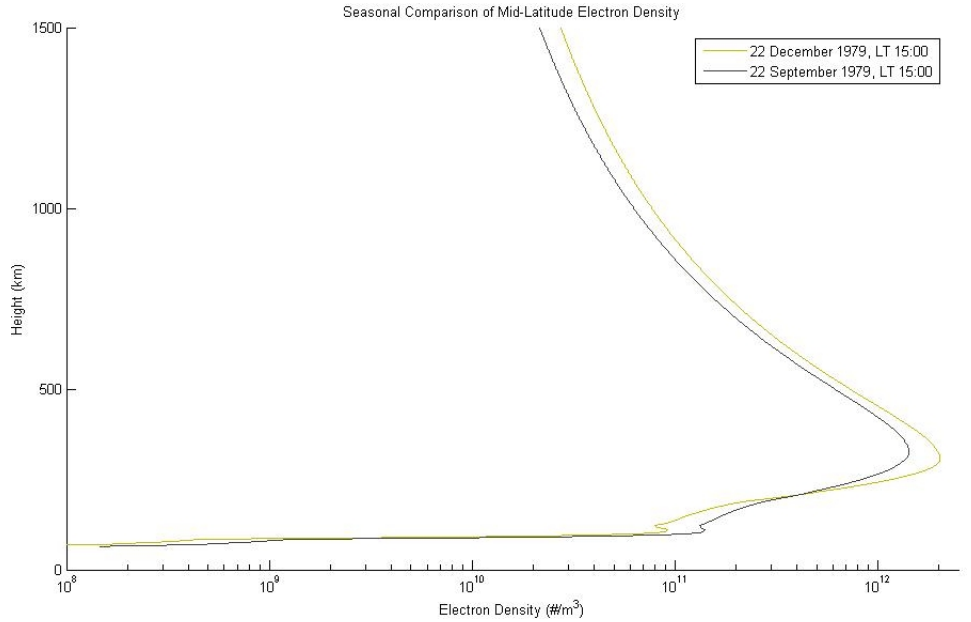

FIG. 2.12 Daytime seasonal variation of electron density for mid-latitude regions.

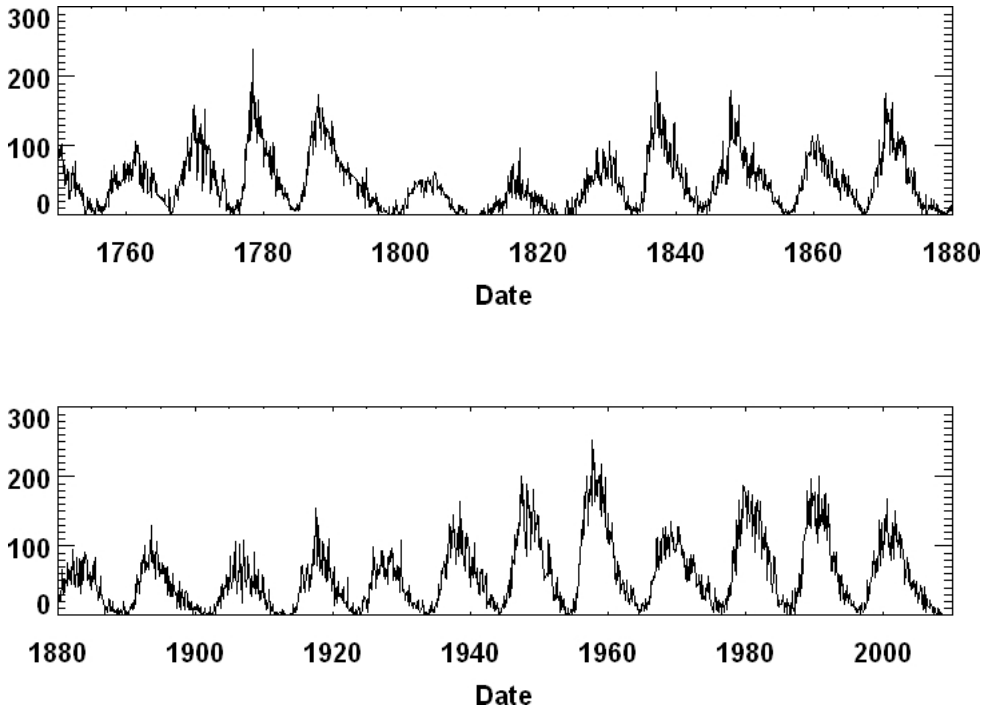

FIG. 2.13 Monthly averages of the International Sunspot Number from 1749 to present [10].

there accordingly exists a strong correlation between the solar cycle and the plasma density. As FIG. 2.14 shows, the F_2 peak density during times of solar maximum can be significantly greater than at times during solar minimum. However, the temperature of the electrons during solar maximum is actually lower than it is at solar minimum. This results from a strong coupling, due to the increased electron density, between the higher-temperature electrons and the lower temperature ions [2].

2.2.3 Sporadic E Layers

Due to the fact that they can occur at any latitude and at any time, Sporadic E Layers, E_s are treated separately. E_s layers are regions of the E layer, usually between 90 and 120 km, which exhibit an increase in plasma density of up to an order of magnitude greater than the surrounding plasma environment [2]. They are usually less than a few kilometers thick, but can be hundreds of kilometers in diameter [9] and can move horizontally between 20-130 m/s [2]. As explained in [2], layers of increased plasma density are formed at high

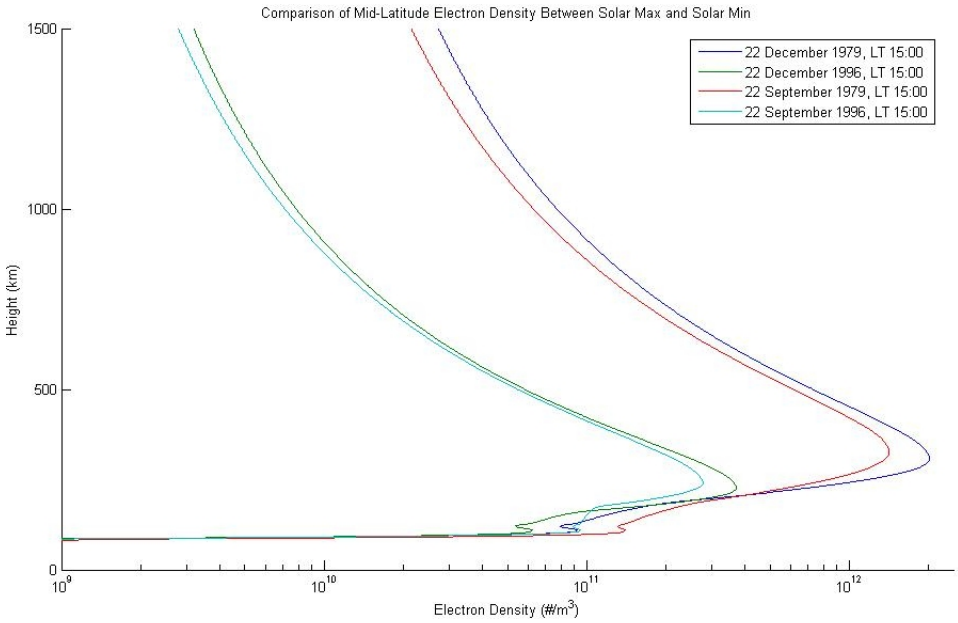

FIG. 2.14 Mid-latitude electron densities during times of solar maximum and minimum.

latitudes by the convection of electric fields, at low-latitudes by gradient instabilities, and at mid-latitudes by wind shears, atmospheric tides, and gravity waves. As metallic ions left from meteorites are concentrated in the E region, these layers of increased plasma densities contain high amounts of Fe^+ and Mg^+ [2]. These metallic ions have a much slower recombination rate than the non-metallic ions and, accordingly, maintain the increased plasma density in the E_s layer. E_s layers can last for several hours [2].

2.3 Expected Ionospheric Conditions

Up to this point, all of the data presented for electron and ion densities and temperatures has been produced by modeling the ionosphere using the IRI. Due to the limited time in which the empirical data sources used by the IRI have been available, the IRI can only be used to model ionospheric conditions since–and including–the year 1958. Upon analysis of the data used for FIG. 2.13 one finds that the extrema in sunspot number from 1958 to the present occur in the years 1979 and 1995, for extremum in solar maxima and minima, respectively (note however, that the maximum sunspot number to occur since measurements

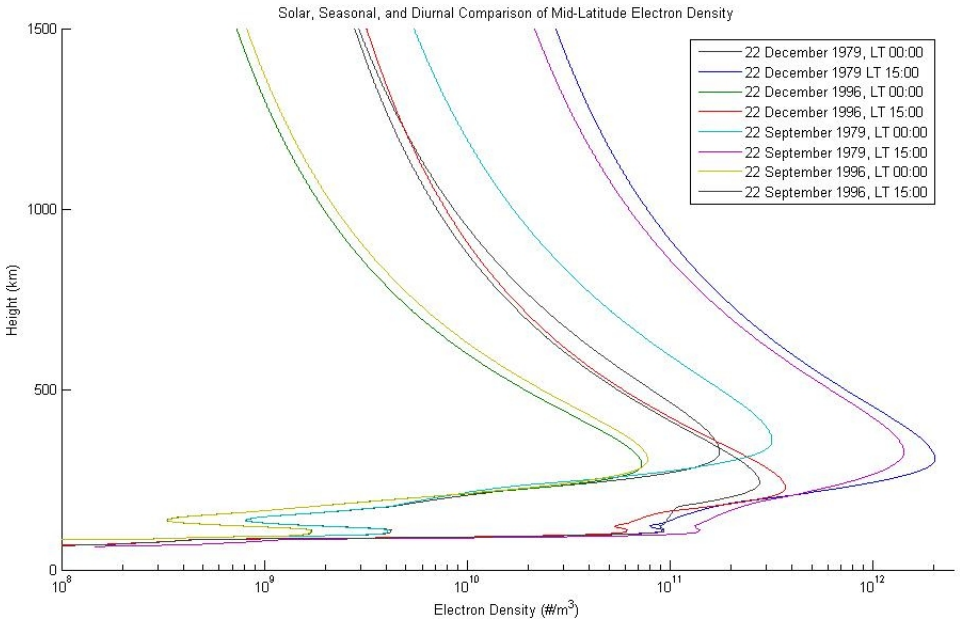

FIG. 2.15 Electron density for various possible ionospheric conditions.

have been taken occurred in October of 1957, where R_i=253.8, but as this was outside of the range of the IRI it could not be modeled). It was for this reason that these years were used to bracket ionospheric conditions. Accordingly, it was found that the maximum in F_2 peak electron density occurred a couple of hours after noon LT during the winter solstice in 1979, while the minimum in F_2 peak electron density occurred a few hours after midnight LT during the summer solstice in 1996. FIG. 2.15 shows the electron density for various temporal conditions during the solstices of solar maximum and minimum while FIG. 2.16 shows the greatest and lowest electron densities exhibited since 1958, as modeled by the IRI. Likewise, the variability and extrema for electron and ion temperatures since 1958, as modeled by the IRI, are shown in Figs. 2.17–2.20.

Although the 2007 IRI code base has many improvements over the previous 2001 code base, it is still not intended to be used to predict ionospheric conditions in auroral regions [11]. Also, whereas the IRI includes a model for geomagnetic storms and the 2007 code base does come with spread F probability prediction, the IRI cannot model ionospheric anomalies such as equatorial bubbles, E_s layers, or substorms. Due to this, the IRI cannot

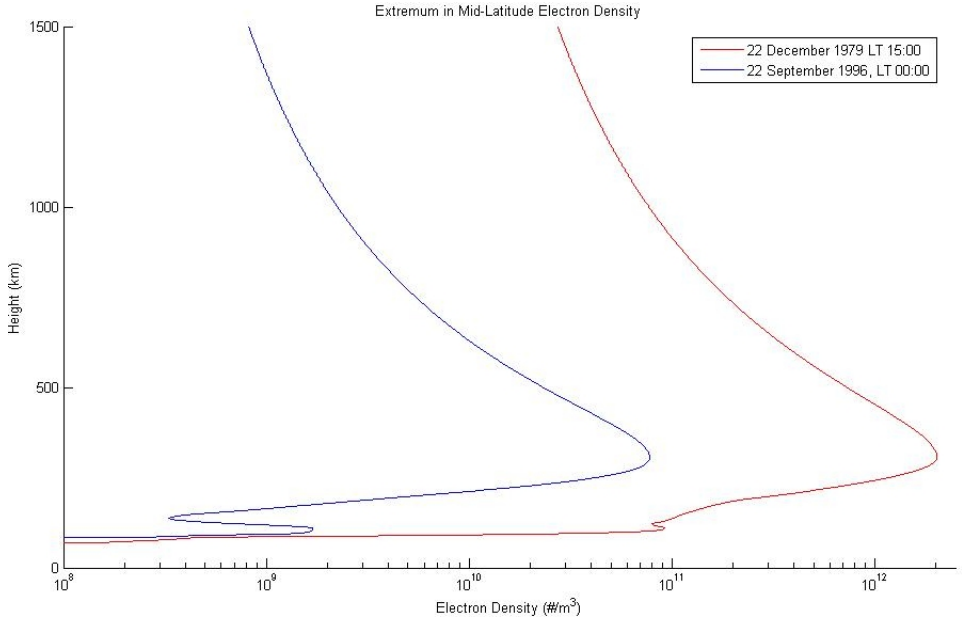

FIG. 2.16 Extemum in electron density for expected worse-case ionospheric conditions.

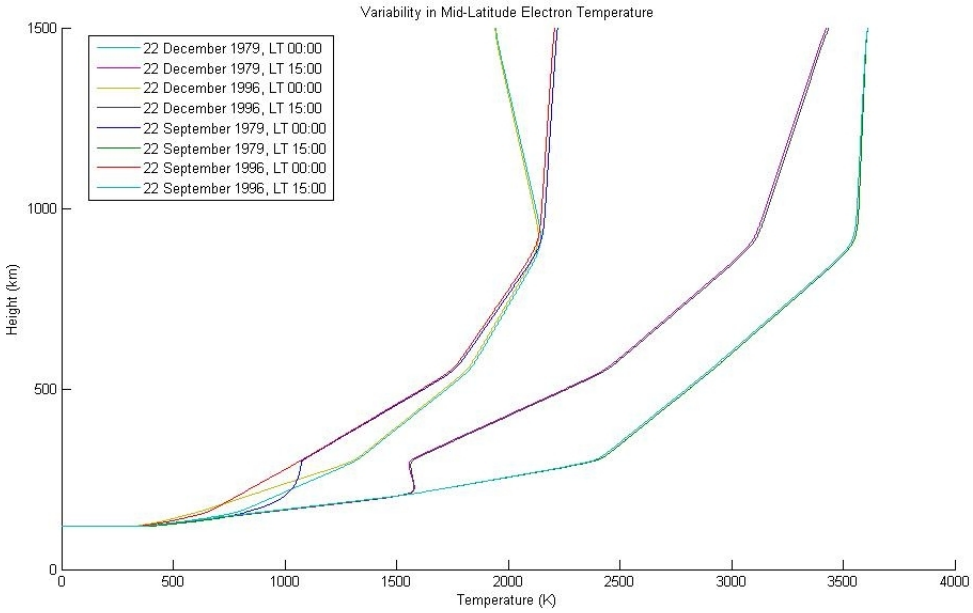

FIG. 2.17 Electron temperature for various possible ionospheric conditions.

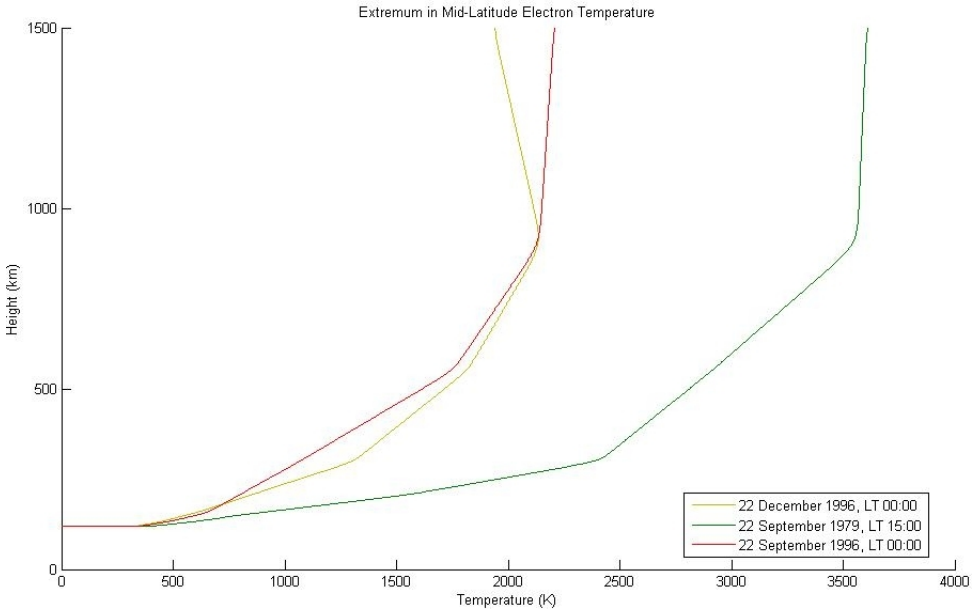

FIG. 2.18 Extemum in electron temperature for expected worse-case ionospheric conditions.

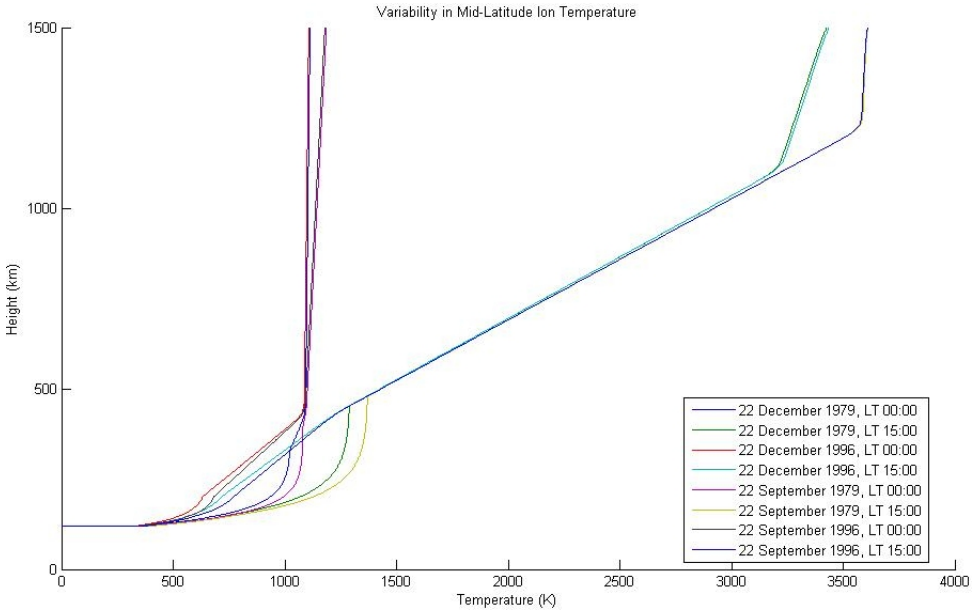

FIG. 2.19 Ion temperature for various possible ionospheric conditions.

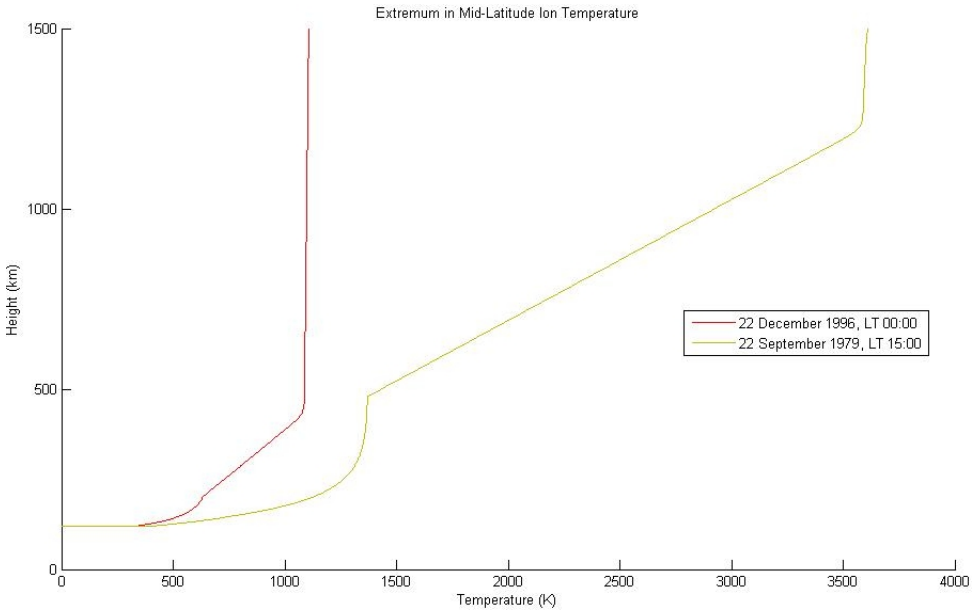

FIG. 2.20 Extemum in ion temperature for expected worse-case ionospheric conditions.

TABLE 2.2 Corrected table of extremum in ionospheric conditions.

	Minimum	Maximum
n_e	$10^8/\mathrm{m}^3$	$10^{13}/\mathrm{m}^3$
n_i	$10^8/\mathrm{m}^3$	$10^13/\mathrm{m}^3$
T_e	300 K	3500 K
T_i	300 K	3500 K

fully model the ionosphere and it is possible for the ionosphere to exhibit characteristics outside of the ranges presented up to this point.

Consequently, it is necessary to estimate how much of an effect these anomalies can have on the modeled data. For this thesis, only mid- to low-lattitude regions are being considered, so short-comings of the IRI for auroral regions can be neglected. However, in the mid- to low-latitude regions, sporatic-E layers can increase the plasma density up to an order of magnitude while plasma bubbles can decrease the plasma density by two orders

of magnitude. Accordingly, Table 2.2 lists the extremum in anticipated electron and ion densities and temperatures for the regions being analyzed by this thesis. As the extremum in plasma density and temperature will end up determining the feasibility of pico-satellite based Langmuir probes hereafter, only these quantities are listed.

CHAPTER 3
LANGMUIR PROBE THEORY

Since the 1920's, Langmuir probes have been used to measure the densities of both electrons and ions (N_e, N_i), as well as the temperature of electrons (T_e) in plasmas [12]. Being first used to measure plasma conditions in laboratory plasma experiments by Mott-Smith and Langmuir, LPs were later adapted to quantify plasma conditions in the Earth's atmosphere [2].

Insofar as measuring atmospheric plasma conditions, a LP consists of a metal plate, cylinder, or sphere that is swept through a range of voltages relative to the satellite ground. As the LP sweeps through these voltages the current between the LP and the satellite's ground is measured. This current is graphed against the voltage of the LP, V_a, producing $I-V$ curves. A typical $I-V$ curve for a spherical LP is shown in FIG. 3.1. Note how this figure is divided into three separate regions. The first region, furthest to the left in the figure, is known as the ion saturation region. Here, the difference between V_a and the plasma voltage, V_p, is negative enough that all thermal electrons in the plasma are repelled from the LP while the ions are accelerated towards the LP. As V_a increases in FIG. 3.1, fewer ions are attracted to the LP while some higher-temperature electrons begin to be collected. As this happens, the transition between the ion saturation region and what is known as the electron retardation region occurs. Within the electron retardation region the slope of the $I-V$ curve is logarthmic, as will be shown hereafter. The point at which the $I-V$ curve is no longer logarthmic marks the transition into the electron saturation region, which consists of V_a being positive enough that electrons are no longer repelled by the LP (although ions may still be collected). From equations derived by Langmuir and others, graphs of the current as a function of voltage for each sweep can be used to find N_e, N_i, and T_e.

3.1 Langmuir Probe Currents

Due to their much lighter mass, the average electron speed in the ionosphere is much higher than that for the ions—even when $T_e \neq T_i$. FIG. 3.2 shows the average velocity of thermal electrons and ions in the ionosphere calculated by using

$$\langle|\overrightarrow{v_{th,j}}|\rangle_M = \left(\frac{8k_B T_j}{\pi m_j}\right)^{1/2} \tag{3.1}$$

for a species j [2], with the approximation $m_i = 16\,\text{amu}$ and the values of T_e and T_i provided by the IRI for 22 September 1979 over Logan, Utah (see FIG. 2.8). Notice that over the range of LEO, the electron velocities can be more than two orders of magnitude greater than ion velocities.

With LEO satellites orbiting at 7–8 km/s relative to the plasma [4], this large velocity difference between the electrons and ions places electrons at supersonic velocities relative to the satellite, while ions remain at subsonic velocities. Due to this, when a satellite is introduced into the plasma environment of the Earth's atmosphere it only collects ram ions, while electrons have a large enough thermal velocity to be collected from all sides.

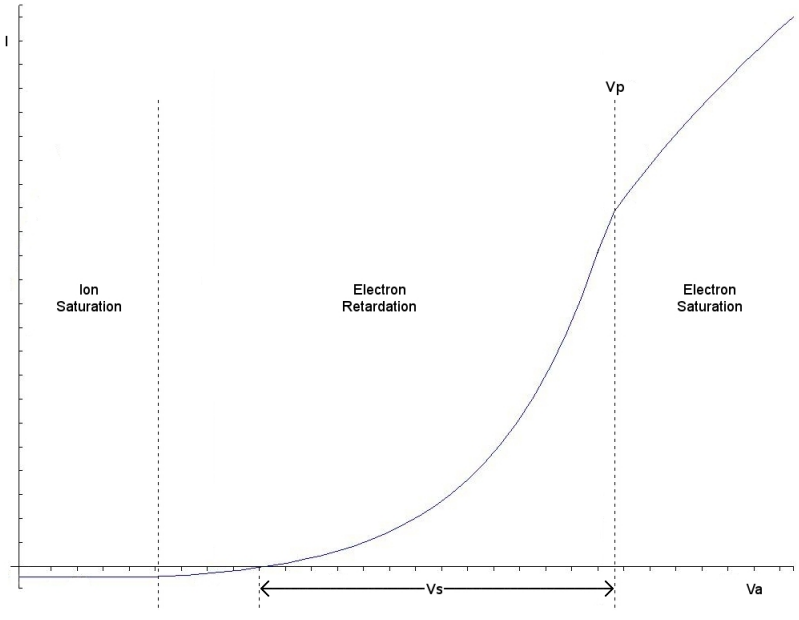

FIG. 3.1 A typical I-V curve, showing the saturation and retardation regions, after [13].

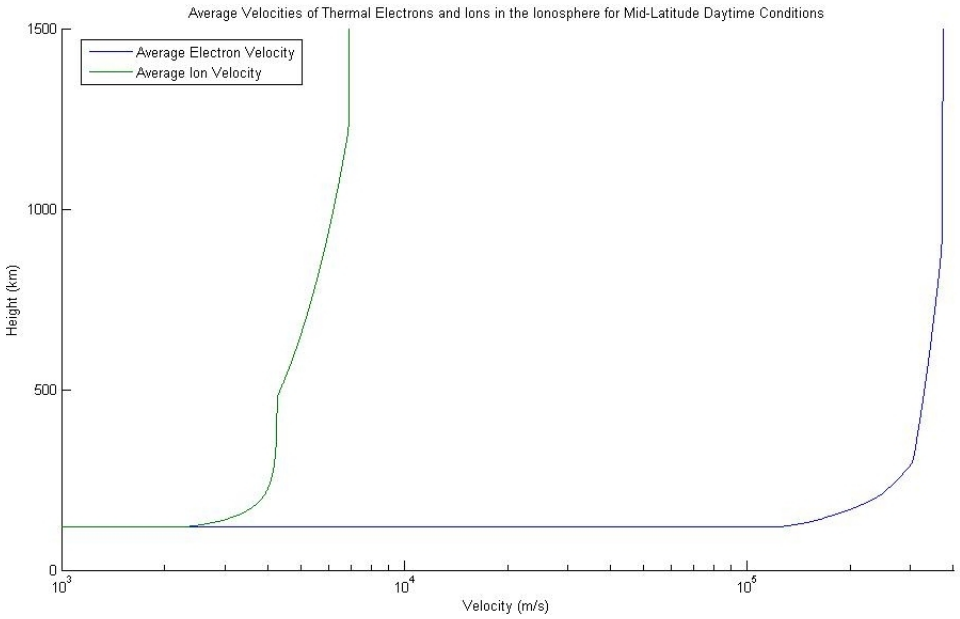

FIG. 3.2 Typical average velocities for thermal electrons and ions in the ionosphere.

Accordingly, as the satellite's conducting surfaces collect both electrons and ions, the surface of the satellite—which is typically referenced as ground—will be driven negative. This satellite voltage, V_s, continues to drop more and more negative, relative to V_p, until the net electric field resulting from the collected electrons on the satellite's surface is sufficient enough to repel further incident thermal electrons. This electric field due to V_s creates an area of positive charge surrounding the satellite, known as the sheath, to the extent that the total amount of positive charge within the sheath is equal to the amount of the net negative charge on the satellite's surface. This sheath extends to several Debye lengths, λ_D, into the plasma [4], where [2]

$$\lambda_D = \left(\frac{\epsilon_0 k_B T_e}{n_e e^2} \right)^{1/2}. \tag{3.2}$$

The sheath which is set up around the satellite, as well as around the LP, is of great importance in LP theory. This is because it is within the sheath that the influence of the electric field of the LP can be seen by the plasma, V_a being effectively shielded by the plasma outside of the sheath. Of particular importance is the relative size of the sheath

with respect to the scale length of the satellite and the LP.

If the characteristic scale length of the LP is much larger than that of the sheath about the LP, then it can be readily assumed that all of the charged particles being accelerated into the sheath by V_a will be collected by the LP. This situation is referred to as the "sheath area limited" [13] or the "thin sheath" [4] case, as the amount of current to the LP is dependent upon the characteristic scale length of the sheath. In this limit, the current to the LP is found by solving Poisson's equation, including both the attracted and repelled particle species [4]. This solution, however, will not be presented here as it is not relavent to the discussion at hand.

The other case occurs when the characteristic scale length of the LP is much smaller than that of the sheath about the LP. In this special case, charged particles being accelerated into the LP sheath by V_a may not be collected by the LP. Instead, particles may pass through the sheath without being collected or become trapped in orbits about the LP and within the sheath. Since the amount of current collected by the LP in this case is determined not only by the effective area of the sheath but also by the angular momentum and energy of the charged particles at the sheath boundary [12], this case is referred to as being "orbital motion limited" (OML) [13] or may also be called the "thick sheath" limit [4]. As shown by FIG. 3.3, typical Debye scales for LEO are on the order of a few cm. Since the size of the sheath is several λ_D and pico-satellites are typically $10\,\mathrm{cm}^3$ or less, the OML case will be that which is applicable to the present study.

The equations describing the amount of current collected in the OML case are given by [13], and can depend on both the region of the $I{-}V$ curve as well as the probe geometry. As was previously mentioned, in the ion saturation region of the $I{-}V$ curves ions are attracted to the LP while thermal electrons are repelled. Accordingly, the current to the LP consists

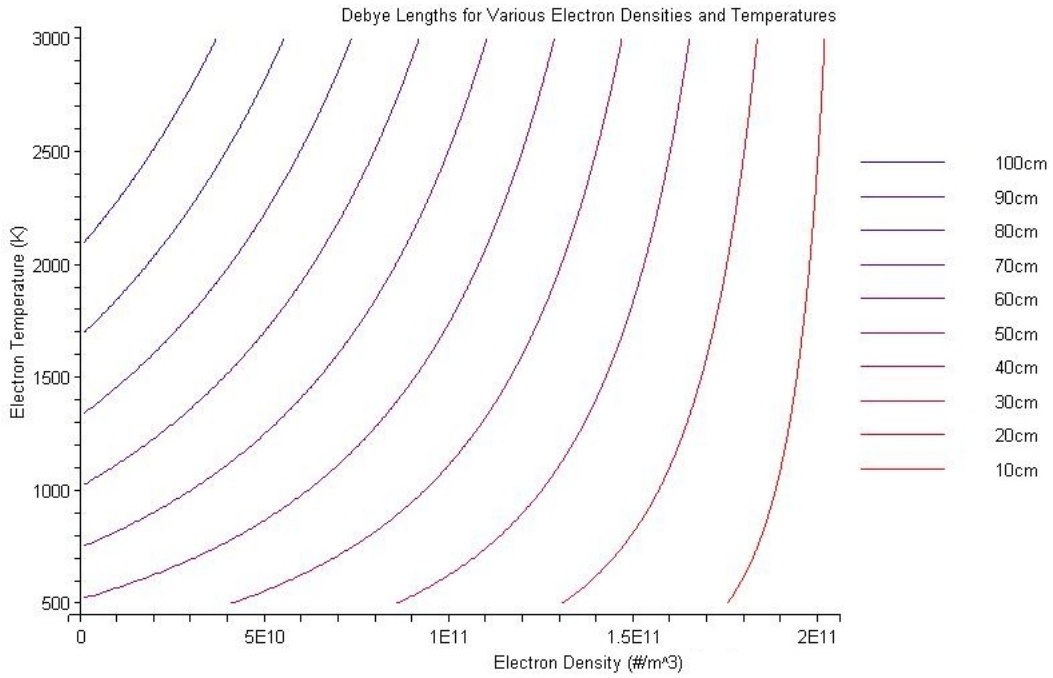

FIG. 3.3 DyBye scales for typical plasma temperatures and densities.

entirely of the ion current [13, 14]

$$I_i(V) = \frac{An_i q_i v_i}{\pi}\left(1+\frac{2k_BT_i}{m_i v_i^2}+\frac{2q_i(V_a-V_p)}{m_i v_i^2}\right)^{\beta} - I_{ph}, \tag{3.3}$$

$$= \frac{An_i|e|v_i}{\pi}\left(1+\frac{2k_BT_i}{m_i v_i^2}+\frac{2|e(V_a-V_p)|}{m_i v_i^2}\right)^{\beta} + |I_{ph}|, \tag{3.4}$$

where

A = the ion collecting surface area of the satellite,

q_i = the ion charge,

v_i = the ion drift velocity relative to the satellite,

m_i = the mean ion mass,

β = 0 for flat plate LPs

= $\frac{1}{2}$ for cylindrical LPs,

= 1 for spherical LPs,

I_{ph} = the photoelectron current.

For these equations and hereafter I have choosen to define current in the traditional way, with positive current being in the direction of anti-electron flow. Accordingly, Eqn. 3.4 explicitly shows the correct signs for such a definition.

Note the three main terms within the parenthesis of Eqns. (3.3) and (3.4). Here, the first term is the contribution of ion current flow to the LP due to the ram ion collection as a result of the ions having subsonic velocities relative to the satellite. In LEO, this term can outweigh the other two terms by an order of magnitude, contributing almost the entire current in the ion saturation region [13]. The second term is the contribution of ion current due to the thermal velocity of the ions. The third term is the current contribution due to the influence of the LP's electric field, V_a, on the ions. Due to the fact that typical LPs have a small cross-sectional area and that the main contribution to the ion saturation current are the ram ions, $I_i(V)$ is usually small.

Also note that the current in the ion saturation region is dependent upon LP geometry. This is true for both of the saturation regions. FIG. 3.1 shows how the choice of probe geometry can influence current collection in these regions. The equations used to generate this graph for the electron retardation and saturation regions are given hereafter.

Within the electron retardation region, the total current to the LP is the resultant of both ion and electron currents. Due to electrons, the current in this region is independent of LP geometry and is given as [13]

$$I_e(V) = An_e q_e \sqrt{\frac{k_B T_e}{2\pi m_e}} \exp\left(\frac{q_e (V_a - V_p)}{k_B T_e}\right) - I_{ph}. \tag{3.5}$$

With the assumption that the ion current in this region is principally due to the ram ion current, the total current in the electron retardation region is

$$I_{total}(V) = n_i|e|A_i v_i + |I_{ph}| - An_e|e|\sqrt{\frac{k_B T_e}{2\pi m_e}} \exp\left(\frac{|e(V_a - V_p)|}{k_B T_e}\right), \tag{3.6}$$

where

$$A_i = \text{the ion collecting ram surface area of the satellite.}$$

Similar to the ions in the ion saturation region, the electrons make the only contribution to the current collected by the LP in the electron saturation region. Since the electrons

have a drift velocity which is supersonic relative to the satellite, the contribution to the current due to the ram electrons is negligible and can be ignored. Therefore, the electron saturation current is a result of only the random electron flux to the LP due to the thermal motion of the electrons and the electron current to the LP due to its electric field, V_a, [13]

$$I_e(V) = \frac{2An_eq_e}{\pi^{1/2}}\left(\frac{k_BT_e}{2\pi m_e}\right)^{1/2}\left(1+\frac{q_e(V_a-V_p)}{k_BT_e}\right)^{\beta} - I_{ph}, \tag{3.7}$$

$$= -\frac{2An_e|e|}{\pi^{1/2}}\left(\frac{k_BT_e}{2\pi m_e}\right)^{1/2}\left(1+\frac{|e(V_a-V_p)|}{k_BT_e}\right)^{\beta} + |I_{ph}|. \tag{3.8}$$

3.2 Deriving Plasma Characteristics

With an understanding of $I-V$ curves and the various currents which contribute to their form, one can derive the values of the parameters N_i, N_e, T_e, V_p, and V_s. To do this, one typically begins by finding the point where the electron retardation region ends and the electron saturation region begins. This provides one with the value of V_p. In removing the contributions to the current collected by the LP due to $n_iq_iA_iv_i$ and I_{ph} in Eqn. (3.6), we are left with an exponential equation for the remaining current collected in the electron retardation region. As neither of the equations for LP current collection in either of the saturation regions are exponential, one can determine the point of separation between the electron retardation region and the electron saturation region by analyzing the $I-V$ curve and finding where it deviates from exponential form. Usually this is done by applying a linear fit to $\ln[I_e(V)]$ versus V_p for the $I-V$ data in the electron retardation region. It can, however, be difficult to determine this point of deviation for spherical probes as the change between these regions is much more subtle than that for other probe geometries, as shown by FIG. 3.4.

Once the deviation from the exponential form of the electron saturation region is determined, the value of V_a for which this occurs is V_p. Further, since no current will flow between the LP and the satellite when they are at the same voltage, the difference between V_p and the value of V_a at which the $I-V$ curve has zero current yields the value of V_s, as shown by FIG. 3.1. From the slope of a linear fit of $\ln[I_e(V)]$ to V_p, one can also determine

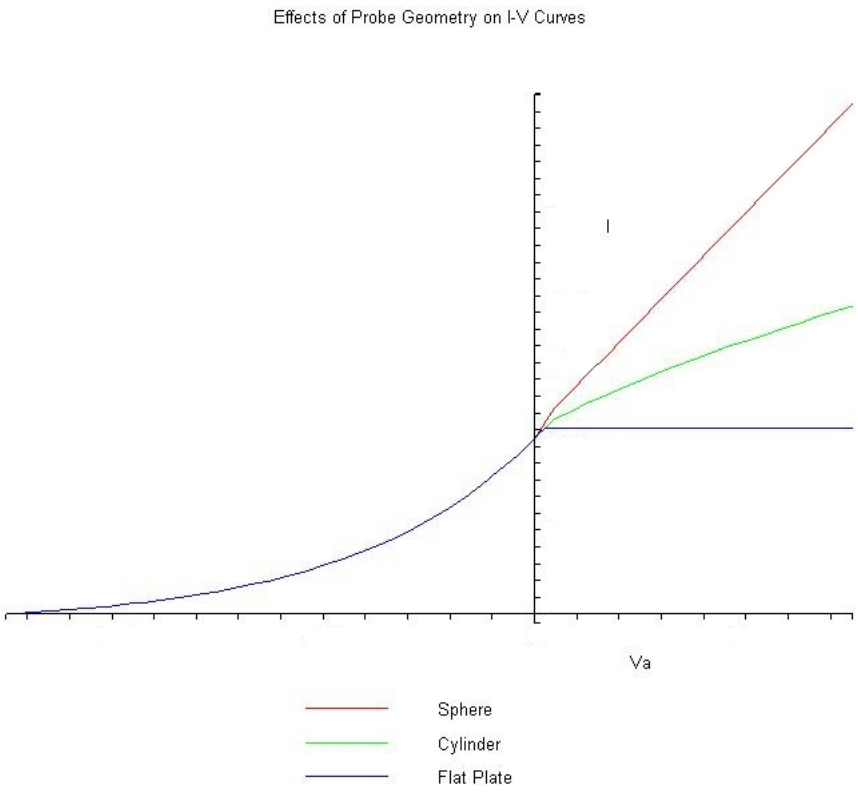

FIG. 3.4 The effects of LP geometry on I-V curves, after [4].

the value of T_e through the relationship [15]

$$\frac{d\left(\ln I_e(V)\right)}{dV_p} = -\frac{e}{k_B T_e}. \tag{3.9}$$

Once the values of V_a, V_p, and T_e are determined, n_e can be readily determined from Eqn. (3.7). Likewise, n_i can be determined from Eqn. (3.7), if a couple of assumptions are made. First, as there are multiple species of ions present in the LEO environment, an average mass for the ions must be assumed. Usually, $m_i = 16\,\text{amu}$ is assumed for F-region altitudes [13]. Secondly, the value of T_i must be known. Typically, in order to calculate N_i from LP data, it is assumed that $T_i = T_e$ [13].

3.3 Limitations in Langmuir Probe Theory

Unfortunately, there are limitations in both LP OML theory and in the practical use of that theory. For instance, in the derivation of the OML equations it was assumed that

the LP collects electrons from all angles. Although the electrons are, in fact, supersonic relative to the satellite, they are not fully collected from the LP wake. Behind the LP there exists a shadow region devoid of ions, due to the fact that the ions are subsonic relative to the satellite. As electrons enter this region, an electric field develops between them and the ions and serves to inhibit electron flow into the wake through ambipolar diffusion [2].

The OML equations as expressed here also do not include the effects of magnetic fields on current collection. Although some progress has been made toward defining the effects of magnetic fields on LP currents for specialized limiting cases, the only way to accurately account for the influence of magnetic fields in general is through Particle-In-Cell (PIC) modeling [16].

The derivation of T_e from the linear fit of $\ln[I_e(V)]$ versus V_p also has its limitations. Here, it is assumed that the plasma has a Maxwellian distribution. If the plasma is not Maxwellian, e.g., if it has a bi-Maxwellian or drifting Maxwellian distribution, the slope of $\ln[I_e(V)]$ versus V_p will not be linear and T_e will not be determinable. Similar, more obvious, limitations arise when determining n_i using the assumptions that $m_i = 16\,\text{amu}$ and $T_i = T_e$. The first of these assumptions, that $m_i = 16\,\text{amu}$, is good for the lower ionosphere where oxygen ions are predominant, but is not as accurate for the topside ionosphere where lighter ion species dominate. The assumption that $T_i = T_e$ is also rather limited, was shown in FIG. 2.8 earlier.

In the application of OML LP theory, there also exist several possible sources of error, as is pointed out by [13]. Some of these sources of error include a non-uniform V_a due to edge effects where cylindrical and spherical LPs attach to their booms and also due to work function patchiness of the surface metal of the LP or due to surface contaminants on the LP. In the former of these two situations, an electrical guard is placed on the end of the boom, near the LP, and electrically isolated from it, and is driven at the same voltage as V_a (in the case of flat plate LPs, which are mounted on the surface of the satellite, the electrical guard consists of an electrically isolated area surrounding all sides of the plate which is also driven at the same voltage of V_a). Although current still cannot be collected where

the boom attaches to the LP, using a guard effectively mitigates edge-field effects. Insofar as the latter of these two situations is concerned, a thin layer of rhenium, molybdenum, gold, or titanium nitride deposited onto the surface of the LP through vapor deposition has been shown to smooth out the work function patchiness [13, 16]. Surface contamination can also be addressed by the careful cleaning and pre-flight storage of LPs, as well as by performing in-flight cleaning through the use of an internal heater (to evaporate away the surface contaminants) or by driving the LP to a large, positive voltage (highly accelerating large numbers of electrons toward the LP and effectively "sand-blasting" off the surface contaminants).

Further limitation in the implementation of LPs can come from the hardware. For instance, if the downlink data rate is not very high, a lower bit size for the $I-V$ data might need to be employed, limiting the number of data points for each V_a sweep. This limited data resolution can make it more difficult to define the point of transition between the electron retardation and electron saturation regions.

However, even with these limitations in the theory and use of LPs, it has been shown by Brace that LPs can still provide 10% accuracy or better on T_e and n_e measurements [13].

CHAPTER 4
PICO-SATELLITE LANGMUIR PROBES

In order for a satellite to remain at a constant floating potential, V_s, it must be able to collect sufficient charge to balance out the charge being collected by the Langmuir probe. If for example, while the Langmuir probe is at the large positive potentials of the electron saturation region, the satellite cannot collect sufficient ions to balance out the net charge of the electrons being collected by the probe, then the satellite potential will be driven negative.

In the previous chapter, the discussion on Langmuir probe theory assumed that the satellite was able to collect sufficient current to balance out the Langmuir probe current and that, as a result, V_s remained relatively constant. Although the effects of a changing V_s on Langmuir probe theory can be discussed [16], it is not the purpose of this thesis to do so. Rather, it will be shown here under what conditions one can can collect sufficient current at the satellite in order to maintain a constant V_s.

4.1 Worst Case Scenario

Of the ion saturation, electron retardation, and electron saturation regions, it is the electron saturation region that presents the most difficult scenario for pico-satellites. The cause of the difficulty is two-fold: first, the velocities of the ions and electrons relative to the satellite are such that the satellite can only collect ram ions while the probe can collect thermal electrons from nearly every side, and second, the large voltage applied to the Langmuir probe also attracts additional electrons.

Accordingly, it becomes necessary to find what ratio between the plasma-collecting surface areas of both the satellite and the Langmuir probe must be maintained in order for the satellite to be able to collect sufficient current to balance out the Langmuir probe current. As the electron retardation and ion saturation regions are less extreme in regards to current collection, we know that if the appropriate area ratio can be found for the electron saturation region that the same ratio can be extended to the other two regions.

For our analysis we need to find what conditions within the electron saturation region give the worst possible scenario. This amounts to collecting the greatest possible current at the Langmuir probe while limiting the collection of ions at the satellite to a realistic minimum. According to Eqn. (3.7), the current collected by the Langmuir probe in the electron saturation region is

$$I(V_a) = -\frac{An_e|e|}{\pi^{1/2}}\left(\frac{2k_BT_e}{\pi m_e} + \frac{2|e(V_a - V_p)|}{\pi m_e}\right)^{\beta} - I_{ph}.$$

As stated earlier, the last term in this equation, I_{ph}, represents the current due to photoelectrons being lost by the probe while it is in sunlight. Thus, I_{ph}, helps lower the net electron collection at the probe and, as we want to consider only the worse case scenario, it will be neglected. The remaining two terms, representing electron currents due to the thermal energy of the electrons and the attraction of the electrons to the Langmuir probe due to its voltage, will be kept. For the total electron current collected by the Langmuir probe, we are therefore left with

$$I(V_a)_{lp} = -\frac{A_{lp}n_e|e|}{\pi^{1/2}}\left(\frac{2k_BT_e}{\pi m_e} + \frac{2|e(V_a - V_p)|}{\pi m_e}\right)^{\beta}, \tag{4.1}$$

where, in order to avoid ambiguity, the electron-collecting surface area of the Langmuir probe has been explicitly labeled A_{lp}. At the satellite, the minimum amount of current collected would simply be that of only the ram ions:

$$I_{sat} = A_{sat}n_i|e|v, \tag{4.2}$$

where A_{sat} represents the ion-collecting area on the ram side of the satellite and v is the velocity of the satellite relative to the ions. In order for V_a to remain constant, we must have that

$$|I_{sat}| = |I(V_a)_{lp}|, \tag{4.3}$$

$$A_{sat}n_i|e|v = \frac{2A_{lp}n_e|e|}{\pi^{1/2}}\left(\frac{k_BT_e}{2\pi m_e}\right)^{1/2}\left(1 + \frac{|e(V_a - V_p)|}{k_BT_e}\right)^{\beta}. \tag{4.4}$$

Solving for the ratio A_{sat}/A_{lp} gives

$$\frac{A_{sat}}{A_{lp}} = \frac{2\left(\frac{k_BT_e}{2\pi m_e}\right)^{1/2}\left(1 + \frac{|e(V_a - V_p)|}{k_BT_e}\right)^{\beta}}{\pi^{1/2}v}, \tag{4.5}$$

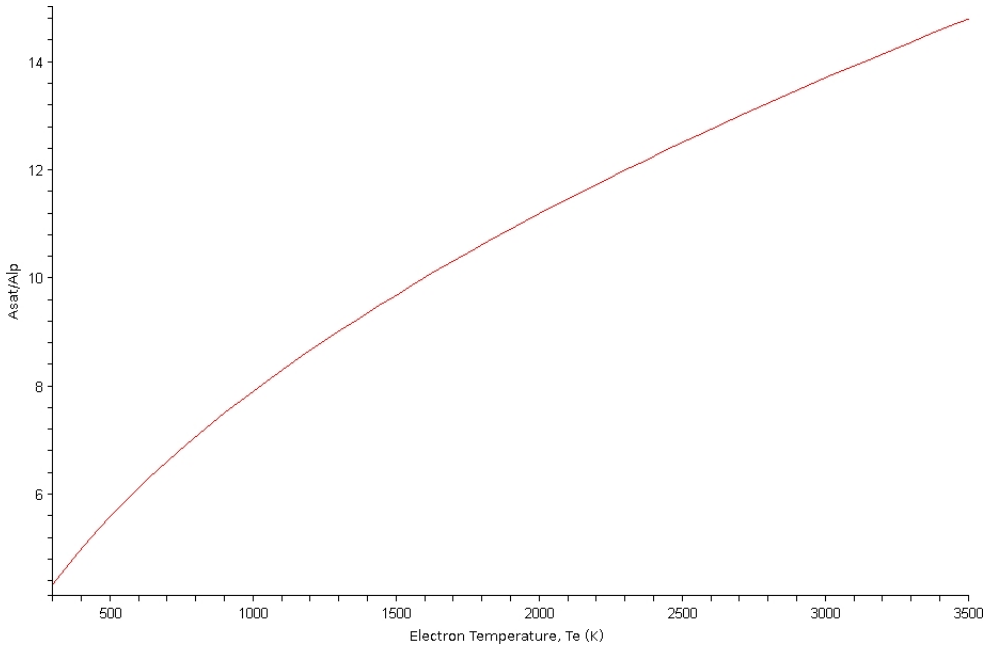

FIG. 4.1 The necessary satellite to probe surface area ratio to prevent a fluctuating satellite potential at the transitional point between the electron retardation and electron saturation regions.

where charge neutrality, $n_e = n_i$, has been assumed.

Note that, according to Eqn. 4.5, the ratio A_{sat}/A_{lp} depends on probe geometry (among other things). With this being this case, subsections 4.1.1–4.1.3 discuss the requirements on A_{sat}/A_{lp} for the saturation regions, as per probe geometry. However, it can be useful to know what A_{sat}/A_{lp} ratio must be maintained in order to keep the satellite voltage constant at the transitional point between the electron retardation region and the electron saturation region. This occurs, by definition, when $V_a = V_p$ and produces the following geometry-independent ratio requirement:

$$\left(\frac{A_{sat}}{A_{lp}}\right)_{V_a=V_p} = \frac{2\left(\frac{k_B T_e}{2\pi m_e}\right)^{1/2}}{\pi^{1/2} v}, \tag{4.6}$$

$$\approx \frac{\sqrt{T_e}}{4}. \tag{4.7}$$

A graph of Eqn. 4.6 is shown in FIG. 4.1. Specifically, for $T_e = 300\,\mathrm{K}$ the ratio $A_{sat}/A_{lp} = 4.336$ must be observed while for $T_e = 3500\,\mathrm{K}$ we must have $A_{sat}/A_{lp} = 14.81$.

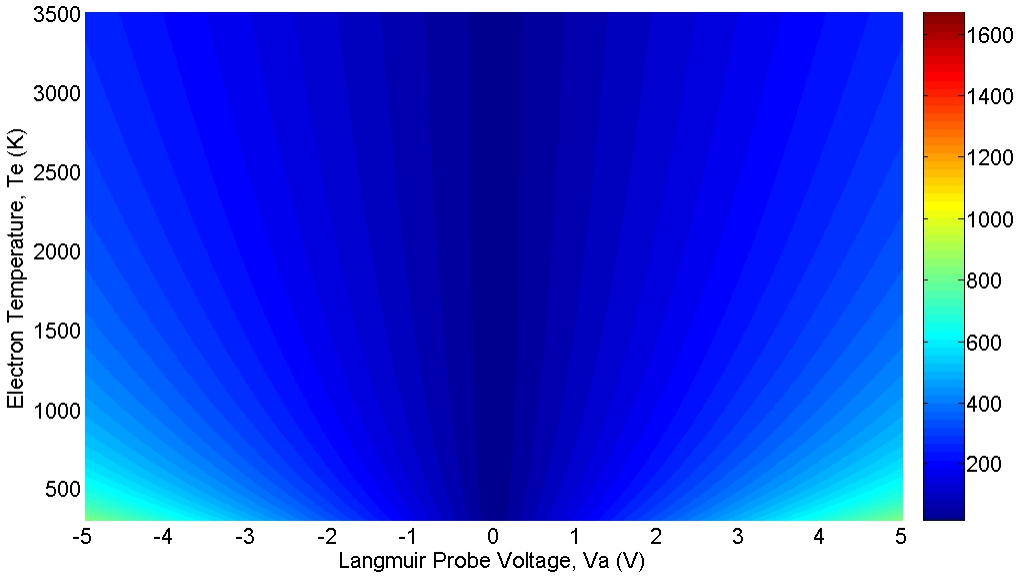

FIG. 4.2 The necessary satellite to probe surface area ratio to prevent a fluctuating V_p for spherical Langmuir probes.

4.1.1 The Spherical Langmuir Probe

Choosing $V_p = 0$, FIG. 4.2 shows the necessary ratio A_{sat}/A_{lp} between the plasma-collecting surface area of a satellite and the surface area of a spherical Langmuir probe that must be maintained for a given T_e and V_a in order to prevent a fluctuating V_p. Note how FIG. 4.2 shows that the necessary ratio A_{sat}/A_{lp} for a spherical probe depends strongly on both T_e and V_a. Specifically, for $V_a = +1\,\mathrm{V}$ and $3500\,\mathrm{K} \geq T_e \geq 300\,\mathrm{K}$, we need the ratios $63.92 \leq A_{sat}/A_{lp} \leq 172.1$. Note that with V_p usually being a few tenths of a volt, $V_a = +1$ V lies within the electron saturation region.

It is interesting to note that, for a given voltage, as T_e increases the ratio A_{sat}/A_{lp} actually decreases. At first appearance, this may seem contrary to logic: with an increase in T_e the thermal electron current would also increase, giving rise to a larger A_{sat}/A_{lp} ratio (i.e., the satellite surface area must increase to allow for the additional collection of ions to counter the increased thermal electron collection at the Langmuir probe). Although this is true, it is not the whole story. As can be seen in Eqn. 4.5, the increase in thermal electron current at the Langmuir probe is proportional to $\sqrt{T_e}$. However, for a spherical Langmuir

probe, with $\beta = 1$, it can also be seen by Eqn. 4.5 that the electron current collection at the Langmuir probe due to the accelerating potential of the probe, V_a, falls off proportional to $1/T_e$. In the resulting product of these terms, $1/T_e$ dominates and the end result is a decreasing A_{sat}/A_{lp} ratio with increasing T_e.

Now, with the necessary A_{sat}/A_{lp} ratio determined, it is useful to find the minimum amount of current that would be generated by a pico-satellite-based Langmuir probe. Since only ram ion current is collected in the ion saturation region, this region which will exhibit the lowest current collection of the saturation regions (the magnitude of the current collection in the electron retardation region falls between those of the saturation regions). If we assume that our pico-satellite is a CubeSat, which measures 10 cm on a side, and if we assume that only one-half of one panel on the CubeSat is available for current collection, then we have that $A_{sat} = 1.333 \times 10^{-5}\ \mathrm{m}^2$. Using the ratio A_{sat}/A_{lp} over the expected range in T_e and V_a and assuming further that only one-half of the probe can collect current (given only ram ions will be collected in the ion saturation region), we can then calculate the Langmuir probe ion saturation current according to

$$I(V_a) = \frac{A_{lp}}{2} n_i |e| v. \tag{4.8}$$

This current is shown in FIG. 4.3. Since the current depends on $n_i = n_e$, the generated current is shown for the extremum in density n_e. Note that at the minimum boundary in density, $n_i = n_e = 10^8/\mathrm{m}^3$, the ion saturation current is on the order of 10^{-13} A, while at the maximum density, $n_i = n_e = 10^{13}/\mathrm{m}^3$, the ion saturation current is on the order of 10^{-8} A. Given the hardware available at the time this thesis was written, it is not unreasonable to assume that currents on the order of 10^{-9} A can be measured. Accordingly, given the assumptions made, ion saturation currents will only be measurable during times of higher ion densities.

However, one can approach the problem from the other direction. For example, if it is desired that a specific ion saturation current—say 5×10^{-9} A—is measured, one can find the necessary minimum spherical Langmuir probe size that must be used to do so. Assuming

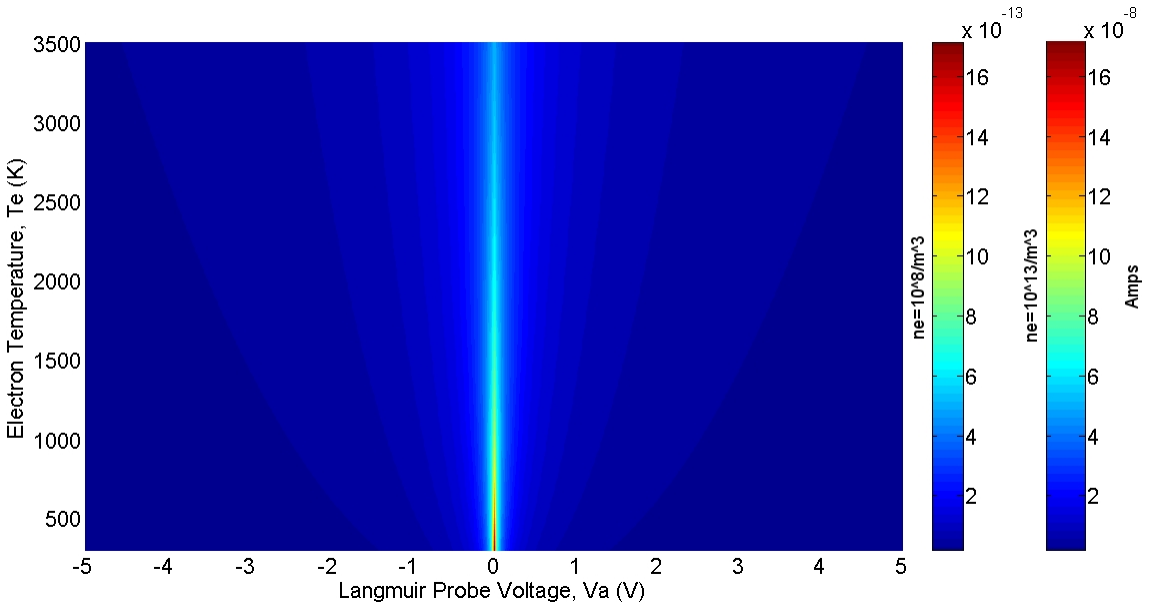

FIG. 4.3 The ion saturation current generated by a spherical Langmuir probe, assuming $A_{sat} = 1.333 \times 10^{-5}\,\mathrm{m}^2$.

TABLE 4.1 The minimum spherical Langmuir probe size required in order to generate at least $5{\times}10^{-9}$ amps of current in the ion saturation region, for various n_i.

Ion Density (#/m^3)	Spherical LP Area (m^2)	Spherical LP Radius (cm)
10^8	8.916×10^{-3}	2.664
10^9	8.916×10^{-4}	0.8423
10^{10}	8.916×10^{-5}	0.2664

that only ram ions are collected for a given density, Table 4.1 gives the necessary minimum spherical Langmuir probe radius required.

For $n_i = 10^8/\mathrm{m}^3$, measuring sufficient ion saturation current is not feasible. However, the probe sizes for measuring ion saturation currents for $n_i \geq 10^9/\mathrm{m}^3$ are within reason.

Recalling that charge neutrality, $n_e = n_i$, is assumed, one might choose to not measure ion saturation currents and simply infer the value of n_i from n_e. In this case, the necessary

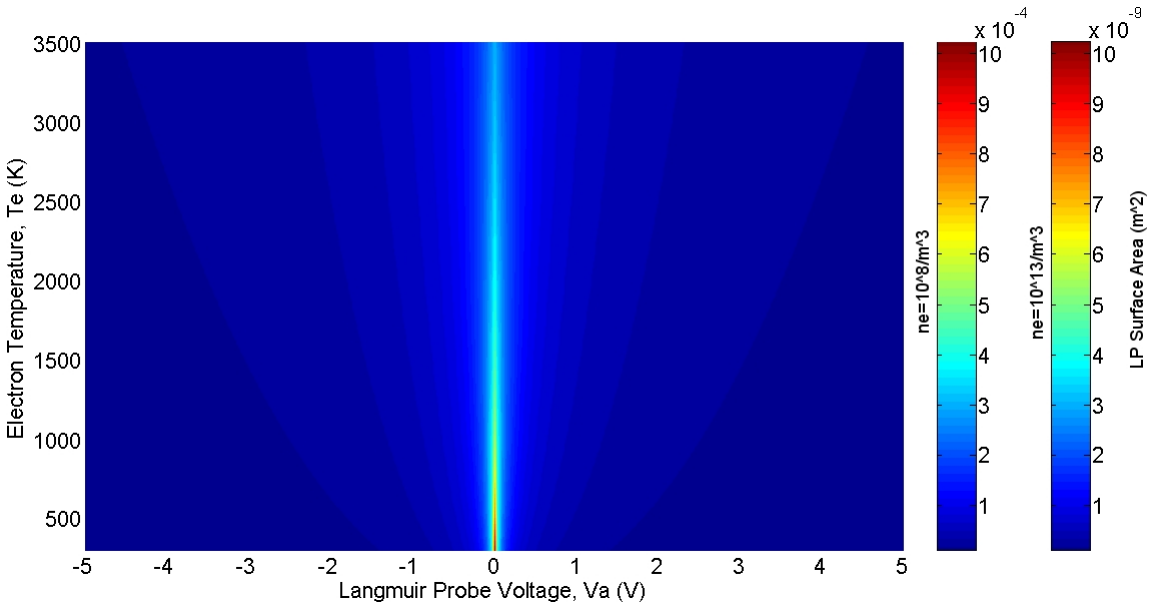

FIG. 4.4 The minimum spherical Langmuir probe surface area required in order to generate at least 5×10^{-9} amps of current in the electron saturation region.

TABLE 4.2 The minimum spherical Langmuir probe size required in order to generate at least 5×10^{-9} amps of current in the electron saturation region, for various n_e.

n_e	T_e	Spherical LP Area	Spherical LP Radius
$(\#/\mathrm{m}^3)$	(K)	(m^2)	(cm)
10^8	300 K	2.591×10^{-5}	1.436×10^{-3}
10^{13}	300 K	2.591×10^{-10}	4.541×10^{-6}
10^8	3500 K	6.975×10^{-5}	2.356×10^{-3}
10^{13}	3500 K	6.975×10^{-10}	7.450×10^{-6}

minimum Langmuir probe size needed to measure 5×10^{-9} A can also be found. FIG. 4.4 shows the necessary probe surface area which must be maintained, for given values of T_e and V_a at the extremum in n_e. Table 4.2 shows what radius the spherical Langmuir probe would need to have in order to measure 5×10^{-9} A for $V_a = +1$ V, given the extremum in n_e.

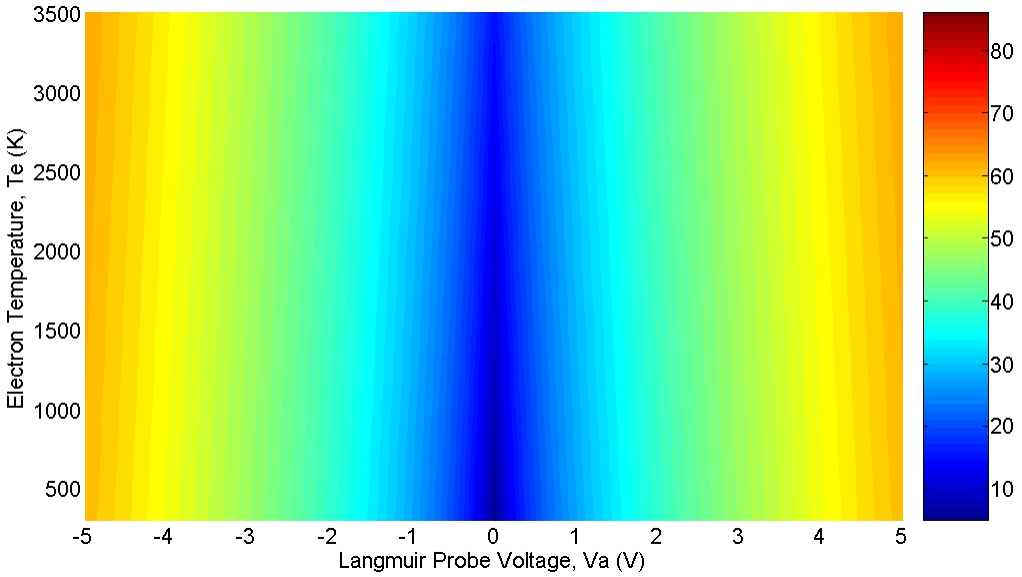

FIG. 4.5 The necessary satellite to probe surface area ratio to prevent a fluctuating V_p for cylindrical Langmuir probes.

As is readily appearent from Table 4.2, measuring electron saturation current does not pose a problem.

4.1.2 The Cylindrical Langmuir Probe

Choosing $V_p = 0$, FIG. 4.5 shows the necessary ratio A_{sat}/A_{lp} between the plasma-collecting surface area of a satellite and the surface area of a cylindrical Langmuir probe that must be maintained for a given T_e and V_a in order to prevent a fluctuating V_p, just as was done for the spherical Langmuir probe. Note that like the spherical Langmuir probe the ratio A_{sat}/A_{lp} for a cylindrical probe depends strongly on V_a, but unlike the spherical probe, the ratio A_{sat}/A_{lp} for a clyindrical probe depends only weakly on T_e. Specifically, for $V_a = +1\,\mathrm{V}$ and $300\,\mathrm{K} \leq T_e \leq 3500\,\mathrm{K}$, we need the ratios $27.32 \leq A_{sat}/A_{lp} \leq 30.77$.

Note that, as one would expect, the ratio A_{sat}/A_{lp} increases with an increasing T_e. This is due to the fact that $\beta = 1/2$ and that the constants associated with each T_e in Eqn. 4.5 lead to an overall increase in the numerator of Eqn. 4.5 as T_e increases.

Having determined the necessary A_{sat}/A_{lp} ratio, we can proceed to find the minimum amount of current that would be generated by a pico-satellite-based cylindrical Langmuir

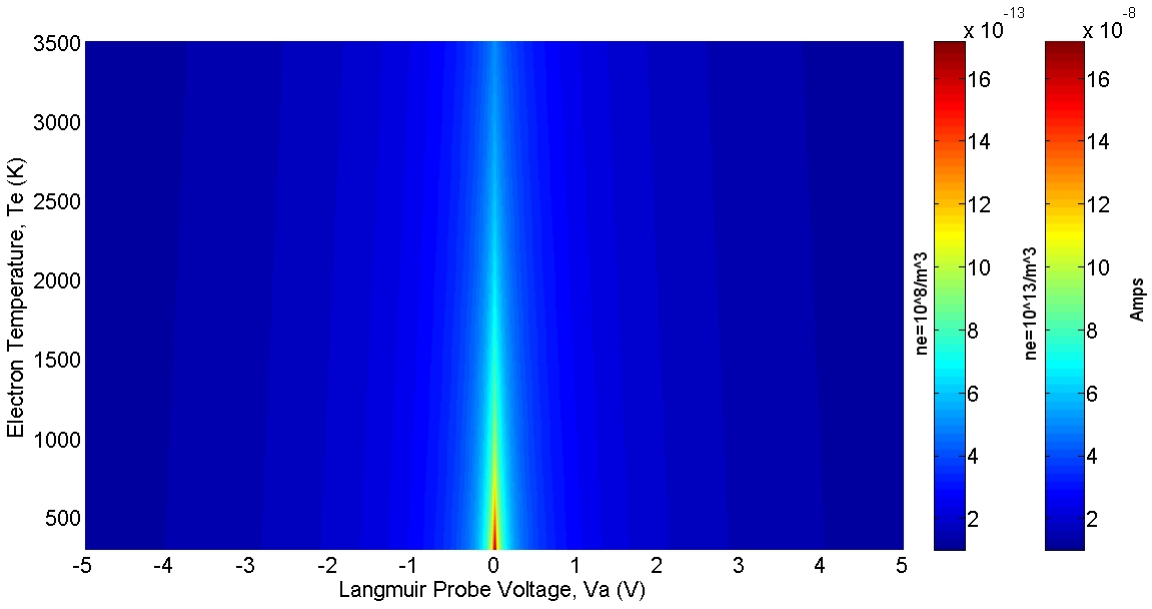

FIG. 4.6 The ion saturation current generated by a cylindrical Langmuir probe, assuming $A_{sat} = 1.333 \times 10^{-5}\,\mathrm{m}^2$.

probe, as was done with the spherical probe. Looking again at the ion saturation current and assuming that our pico-satellite is a CubeSat with only one-half of one panel available for current collection, we can calculate the ion saturation current for a cylindrical Langmuir probe.

This current is shown in FIG. 4.6. Since the current depends on $n_i = n_e$, the generated current is shown for the extremum in density n_e. Note that at the minimum boundary in density, $n_i = n_e = 10^8/\mathrm{m}^3$, the ion saturation current is on the order of $10^{-13}\,\mathrm{A}$, while at the maximum density, $n_i = n_e = 10^{13}/\mathrm{m}^3$, the ion saturation current is on the order of 10^{-8} A (recall that the spherical probe demonstrated same magnitude in ion saturation current as is shown here for the cylindrical probe). Accordingly, given the assumptions made, ion saturation currents will only be measurable during times of higher ion densities, just as was found for the spherical probe.

Approaching the problem from the other direction, and assuming again that an ion saturation current of $5 \times 10^{-9}\,\mathrm{A}$ is desired to be measured, one can find the necessary minimum cylindrical Langmuir probe size that must be used in order to do so. Assuming that only

TABLE 4.3 The minimum cylindrical Langmuir probe size required in order to generate at least 5×10^{-9} amps of current in the ion saturation region, for various n_i.

Ion Density ($\#/m^3$)	Cylindrical LP Area (m^2)	Cylindrical LP Length (cm)
10^8	8.916×10^{-3}	141.9
10^9	8.916×10^{-4}	14.19
10^{10}	8.916×10^{-5}	1.419

ram ions are collected for a given density, Table 4.3 gives the necessary minimum cylindrical Langmuir probe radius required. Note that for these calculations a probe diameter of 0.2 cm has been assumed.

For $n_i = 10^8/m^3$, measuring sufficient ion saturation current is not feasible with the cylindrical Langmuir probe. However, the probe sizes for measuring ion saturation currents for $n_i \geq 10^9/m^3$ are within reason.

The minimum cylindrical probe size that must be used in order to measure 5×10^{-9} A in the electron saturation region can also be found, just as was done for the spherical probe. FIG. 4.7 shows the necessary probe surface area which must be maintained, for given values of T_e and V_a at the extremum in n_e. Table 4.4 shows what length the cylindrical Langmuir probe would need to have in order to measure 5×10^{-9} A for $V_a = +1$ V, given the extremum in n_e (again assuming a probe diameter of 0.2 cm).

As is readily apparent from Table 4.4, measuring electron saturation current does not pose a problem.

4.1.3 The Flat Plate Langmuir Probe

Choosing $V_p = 0$, FIG. 4.8 shows the necessary ratio A_{sat}/A_{lp} between the plasma-collecting surface area of a satellite and the surface area of a flat plate Langmuir probe that must be maintained for a given T_e and V_a in order to prevent a fluctuating V_p, just as was

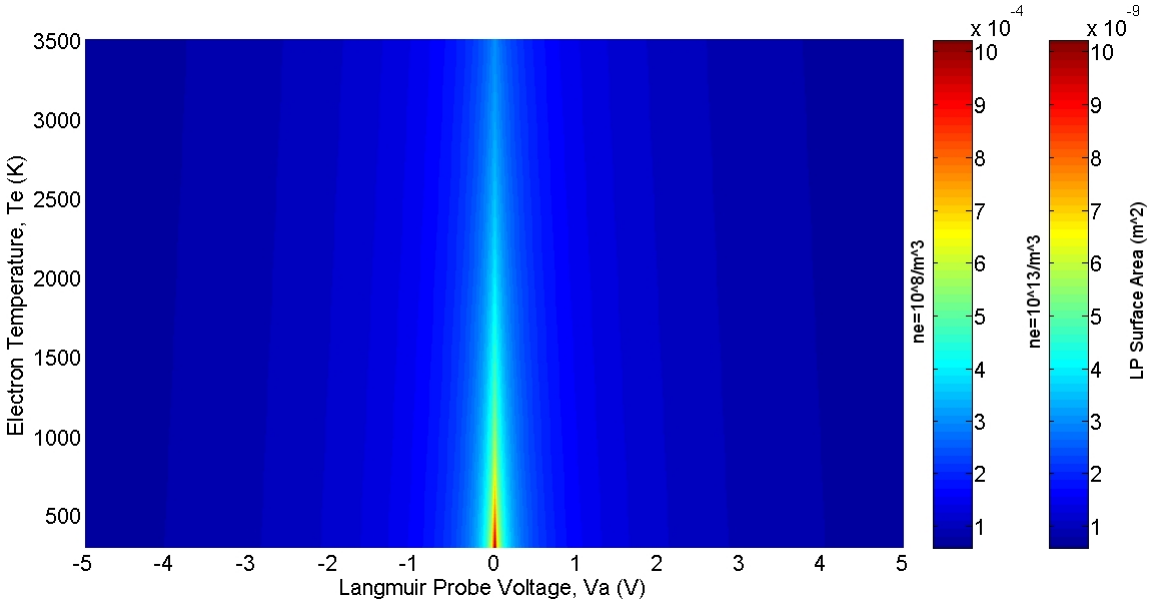

FIG. 4.7 The minimum cylindrical Langmuir probe surface area required in order to generate at least 5×10^{-9} amps of current in the electron saturation region.

TABLE 4.4 The minimum cylindrical Langmuir probe size required in order to generate at least 5×10^{-9} amps of current in the electron saturation region, for various n_e.

n_e	T_e	Cylindrical LP Area	Cylindrical LP Length
$(\#/\mathrm{m}^3)$	(K)	(m^2)	(cm)
10^8	300 K	5.054×10^{-5}	4.022×10^{-3}
10^{13}	300 K	5.054×10^{-10}	4.022×10^{-8}
10^8	3500 K	1.133×10^{-4}	9.016×10^{-3}
10^{13}	3500 K	1.133×10^{-9}	9.016×10^{-8}

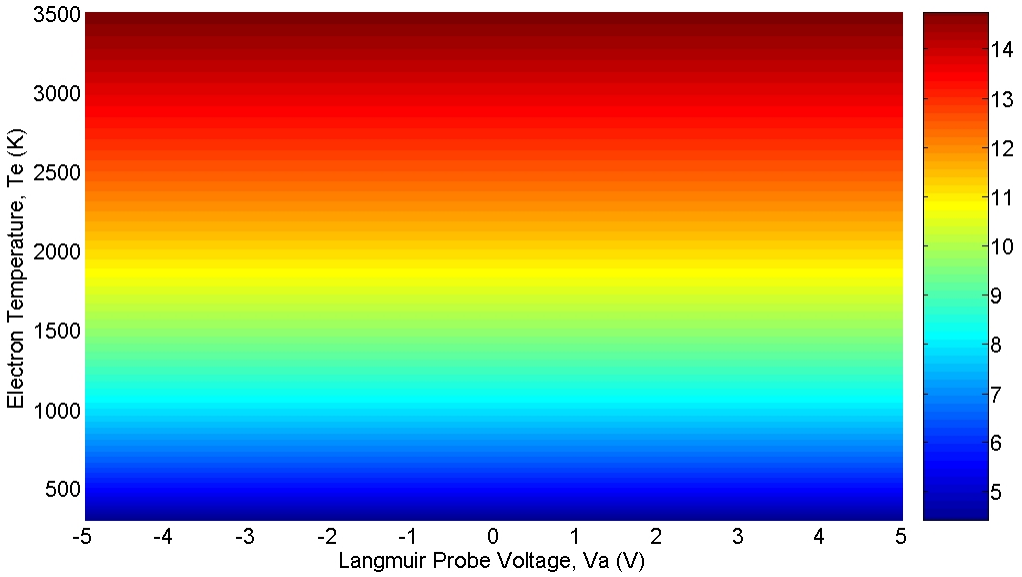

FIG. 4.8 The necessary satellite to probe surface area ratio to prevent a fluctuating V_p for flat plate Langmuir probes.

done for the spherical and cylindrical Langmuir probes. Note that unlike either the spherical or cylindrical Langmuir probes, the ratio A_{sat}/A_{lp} for a flat plate probe depends entirely on T_e. This is due to the fact that $\beta = 0$ in Eqn. 4.5, eleminating the V_a dependence. Here, as with the cylindrical Langmuir probe, the ratio A_{sat}/A_{lp} increases with an increasing T_e. Specifically, we show that for $V_a = +1$ V, $A_{sat}/A_{lp} = 4.336$ and $A_{sat}/A_{lp} = 14.81$, and $T_e = 300\,\mathrm{K}$ and $T_e = 3500\,\mathrm{K}$, respectively.

Having determined the necessary A_{sat}/A_{lp} ratio, we can proceed to find the minimum amount of current that would be generated by a pico-satellite-based flat plate Langmuir probe, as was done with the spherical and cylindrical probes. Looking again at the ion saturation current and assuming that our pico-satellite is a CubeSat with only one-half of one panel available for current collection, we can calculate the ion saturation current for a flat plate Langmuir probe. This current is shown in FIG. 4.9. Since the current depends on $n_i = n_e$, the generated current is shown for the extremum in density n_e. Note that at the minimum boundary in density, $n_i = n_e = 10^8/\mathrm{m}^3$, the ion saturation current is on the order of 10^{-12} A, while at the maximum density, $n_i = n_e = 10^{13}/\mathrm{m}^3$, the ion saturation

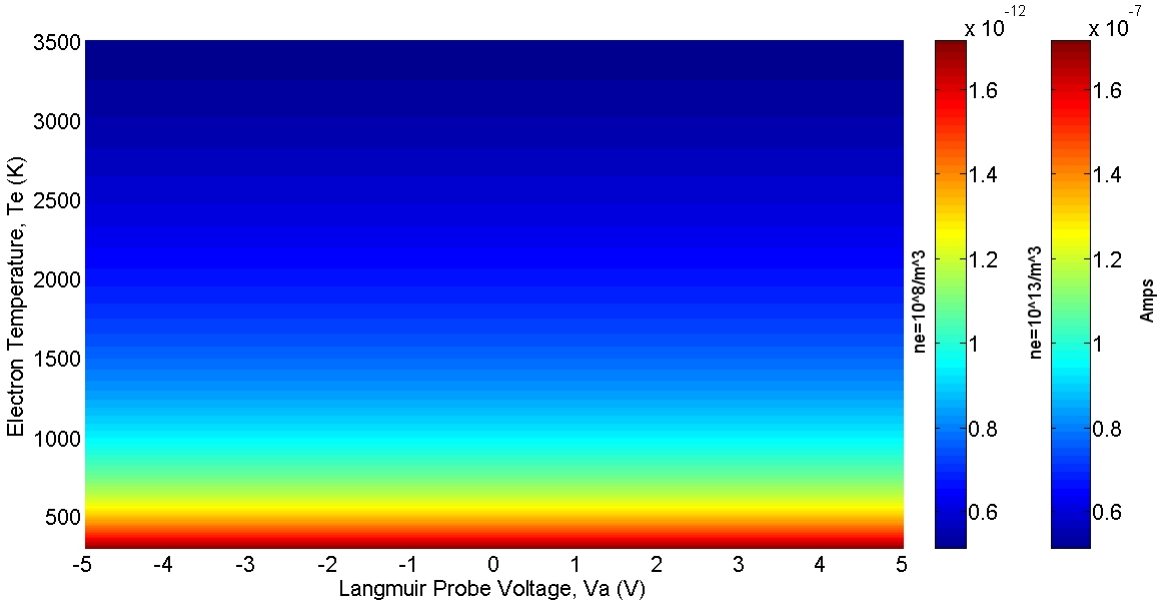

FIG. 4.9 The ion saturation current generated by a flat plate Langmuir probe, assuming $A_{sat} = 1.333 \times 10^{-5}\,\mathrm{m}^2$.

current, is on the order of $10^{-7}\,\mathrm{A}$ (recalling that each of these ion saturation currents are an order of magnitude greater than those of the spherical or cylindrical probes). Still, given the assumptions made, ion saturation currents will only be measurable during times of higher ion densities, just as was found for the spherical and cylindrical probes.

Approaching the problem from the other direction, and assuming again an ion saturation current of $5 \times 10^{-9}\,\mathrm{A}$ is to be measured, one can find the necessary minimum flat plate Langmuir probe size that must be used in order to do so. Assuming that only ram ions are collected for a given density, Table 4.5 gives the necessary minimum flat plate Langmuir probe radius required. Note that for these calculations a square flat plate Langmuir probe has been assumed.

For $n_i = 10^8/\mathrm{m}^3$, measuring sufficient ion saturation current is not feasible with the flat plate Langmuir probe (recall that CubeSats measure only 10 cm on a side). However, the probe sizes for measuring ion saturation currents for $n_i \geq 10^9/\mathrm{m}^3$ are within reason.

The minimum flat plate probe size that must be used in order to measure $5 \times 10^{-9}\,\mathrm{A}$ in the electron saturation region can also be found, just as was done for the spherical

TABLE 4.5 The minimum flat plate Langmuir probe size required in order to generate at least 5×10^{-9} amps of current in the ion saturation region, for various n_i.

Ion Density (#/m^3)	Flat Plate LP Area (m^2)	Flat Plate LP Side (cm)
10^8	8.916×10^{-3}	9.443
10^9	8.916×10^{-4}	2.986
10^{10}	8.916×10^{-5}	0.9443

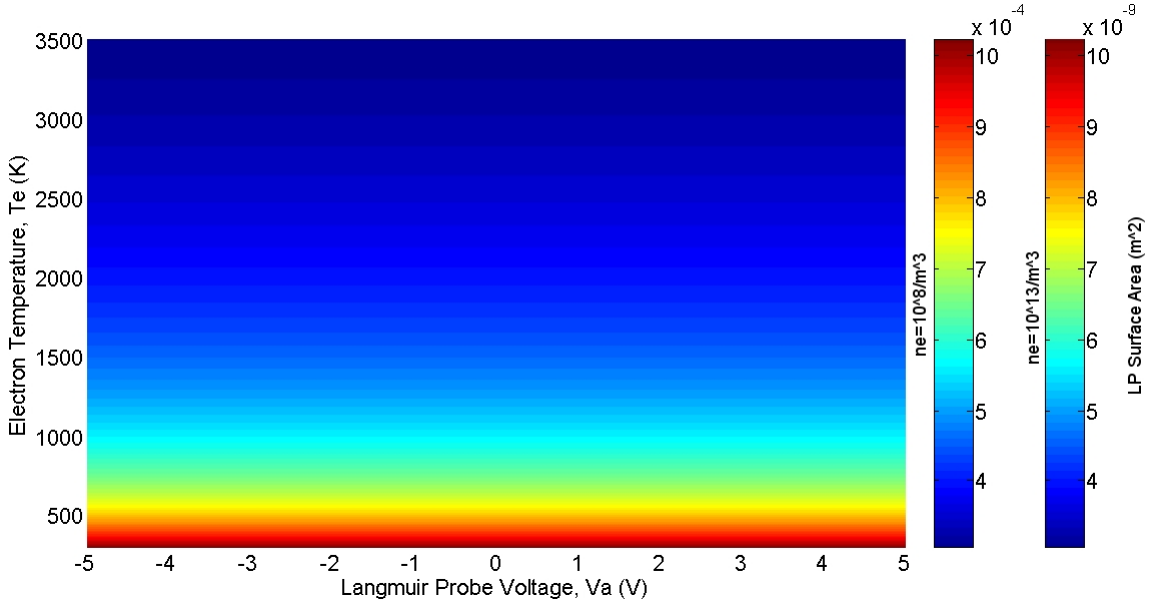

FIG. 4.10 The minimum flat plate Langmuir probe surface area required in order to generate at least 5×10^{-9} amps of current in the electron saturation region.

and cylindrical probes. FIG. 4.10 shows the necessary probe surface area which must be maintained, for a given value of T_e at the extremum in n_e. Table 4.6 shows what side length the flat plate Langmuir probe would need to have in order to measure 5×10^{-9} A, given the extremum in n_e.

As is readily apparent from Table 4.6, measuring electron saturation current does not pose a problem.

TABLE 4.6 The minimum flat plate Langmuir probe size required in order to generate at least 5×10^{-9} amps of current in the electron saturation region, for various n_e.

n_e	T_e	Flat Plate LP Area	Flat Plate LP Side Length
$(\#/m^3)$	(K)	(m^2)	(cm)
10^8	300 K	1.028×10^{-3}	3.206×10^{-2}
10^{13}	300 K	1.028×10^{-8}	1.014×10^{-4}
10^8	3500 K	3.010×10^{-4}	1.735×10^{-2}
10^{13}	3500 K	3.010×10^{-9}	5.486×10^{-5}

4.2 Other Considerations

As was discussed in the previous chapter, including the additional current terms in OML Langmuir probe theory helps prevent V_{sat} fluctuations in the ion saturation region. However, the OML theory presented here does not account for the effects on current collection when the plasma is magnetized, such as is the case with Earth's ionosphere. Fortunately, having a magnetized plasma ends up limiting the amount of electrons that can be collected by the Langmuir probe. Accordingly, including the effects of magnetic fields on the plasma only serves to help prevent V_{sat} fluctuations in the ion saturation region.

Also, the OML theory presented here does not account for ambipolar diffusion, which limits the amount of electrons that can be collected by the Langmuir probe and satellite in their wakes. Limiting the electron current collection at the Langmuir probe due to ambipolar diffusion, results in requiring a lower ion current collection being needed at the satellite in order to prevent V_{sat} fluctuations in the ion saturation region. Additionally, in the ion saturation region there will still be sufficient electron current collection at the satellite in order to balance out the ion current being collected by the Langmuir probe.

Finally, due to their characteristic scale length in comparison to the Debye lengths found in the ionosphere, it might be argued that current collection at a pico-satellite itself needs to be modeled after OML theory. However, doing so would not have an effect on

collecting sufficient ion current at the satellite in order to balance out the electron current collected at the Langmuir probe in the electron saturation region, as only ram ion current is being assumed to be collected. In the ion saturation region, much like in case of ambipolar diffusion, it will still be possible to collect sufficient electron current at the satellite in order to balance out the ion current being collected at the Langmuir probe.

In summary, using a Langmuir probe to measure ion saturation currents in ionospheric regions with an ion density lower than $10^9/\mathrm{m}^3$ would not be readily feasible with a 1U CubeSat. However, this would be feasible with satellites on the order of a 3U CubeSat. Still, even if the satellite size prohibits the measurements of ion saturation currents at lower plasma densities, it is possible to measure electron retardation and saturation currents, thereby providing measurements for T_e, n_e, and V_p. Since the plasma is assumed to be charge nuetral, one can use n_e to estimate n_i, allowing for the use of pico-satellite-based Langmuir probes for mid- to low-lattitude LEO missions.

CHAPTER 5
CONCLUSION

In conclusion, it has been shown that it is possible to use Langmuir probes on pico-satellites to measure ionospheric plasma quantities for mid- to low-latitude LEO missions. These calculations were based on orbital motion limited Langmuir probe theory according to the assumptions that, for these regions and orbits, the extremum in plasma density would be $10^8/\mathrm{m}^3 \leq n_e, n_i \leq 10^{13}/\mathrm{m}^3$, while the extremum in plasma temperature would be $300\,\mathrm{K} \leq T_e, T_i \leq 3500\,\mathrm{K}$.

Specifically, it was found that the necessary ratio, A_{sat}/A_{lp}, between the plasma-collecting surface area of the satellite and the surface area of the Langmuir probe depended greatly on probe geometry. For the spherical Langmuir probe, A_{sat}/A_{lp} depended stongly on both T_e and V_a, with $63.92 \leq A_{sat}/A_{lp} \leq 172.1$ for $3500\,\mathrm{K} \geq T_e \geq 300\,\mathrm{K}$. For the cylindrical probe, A_{sat}/A_{lp} was found to depend strongly on V_a with $27.32 \leq A_{sat}/A_{lp} \leq 30.77$ for $300\,\mathrm{K} \leq T_e \leq 3500\,\mathrm{K}$. For the flat plate probe, it was shown that A_{sat}/A_{lp} depends only on T_e with $A_{sat}/A_{lp} = 4.336$ for $T_e = 300\,\mathrm{K}$ and $A_{sat}/A_{lp} = 14.81$ for $T_e = 3500\,\mathrm{K}$. Aditionally, the minimum ion saturation currents generated in using the minimum ratio for A_{sat}/A_{lp} were determined for each probe geometry, with the assumption that only $1.333 \times 10^{-5}\,\mathrm{m}^2$ of the satellite's surface is available for plasma collection and that only one-half of the Langmuir probe's surface area is available for ion saturation current collection. The orders of magnitude for these ion saturation current values are presented in Table 5.1. The necessary probe sizes needed in order to generate a minimum of 5×10^{-9} amps, for both of the electron and ion saturation regions, were also determined and are presented again in Tables 5.2–5.3. It was also determined that the necessary A_{sat}/A_{lp} ratio which must be maintained in order to keep the satellite voltage constant at the transitional point between the electron retardation region and the electron saturation region is $A_{sat}/A_{lp} = 4.336$ for $T_e = 300\,\mathrm{K}$ and $A_{sat}/A_{lp} = 14.81$ for $T_e = 3500\,\mathrm{K}$.

TABLE 5.1 The maximum attainable ion saturation current, assuming $A_{sat} = 1.333 \times 10^{-5}$ m^2, for pico-satellite-based Langmuir probes used on mid- to low-lattitude LEO missions.

n_i (#/m^3)	Spherical LP (A)	Cylindrical LP (A)	Flat Plate LP (A)
10^8	10^{-13}	10^{-13}	10^{-12}
10^{13}	10^{-8}	10^{-8}	10^{-7}

TABLE 5.2 Minimum Langmuir probe dimensions necessary in order to generate at least 5×10^{-9} A of current in the ion saturation region, at the extremum in plasma density.

n_i (#/m^3)	LP Area (m^2)	Spherical LP (radius, cm)	Cylindrical LP (length, cm)	Flat Plate LP (side, cm)
10^8	8.916×10^{-3}	2.664	141.9	9.443
10^9	8.916×10^{-4}	0.8423	14.19	2.986
10^{10}	8.916×10^{-5}	0.2664	1.419	0.9433

TABLE 5.3 Minimum Langmuir probe dimensions necessary in order to generate at least 5×10^{-9} A of current in the electron saturation region, at the extremum in plasma density.

n_e (#/m^3)	T_e (K)	Spherical LP (radius, cm)	Cylindrical LP (length, cm)	Flat Plate LP (side, cm)
10^8	300	1.436×10^{-3}	4.022×10^{-3}	3.206×10^{-2}
10^{13}	3500	4.541×10^{-6}	4.022×10^{-8}	1.014×10^{-4}
10^8	300	2.356×10^{-3}	9.016×10^{-3}	1.735×10^{-2}
10^{13}	3500	7.450×10^{-6}	9.016×10^{-8}	5.486×10^{-5}

REFERENCES

[1] SSHP, http://centaur.sstl.co.uk/SSHP/sshp_classify.html.

[2] R. W. Schunk *et al.*, *Ionospheres-Physics, Plasma Physics, and Chemistry* (Cambridge University Press, Cambridge, 2000).

[3] Virgin Galactic, http://www.virgingalactic.com.

[4] D. Hastings *et al.*, *Spacecraft-Environment Interactions* (Cambridge University Press, Cambridge, 1996).

[5] A. Brekke, *Physics of the Upper Polar Atmosphere* (Wiley, New York, 1997).

[6] H. A. Bekerat, *Evaluation of Plasma Convection Models and Their Effect on the High-Latitude Ionosphere* (Utah State University, Logan, 2006).

[7] NASA, http://iri.gsfc.nasa.gov/.

[8] ATIS, http://www.atis.org/glossary/.

[9] T. F. Tascione, *Introduction to the Space Environment* (Orbit Book Company, Malabar, 1988).

[10] MSFC, http://solarscience.msfc.nasa.gov/SunspotCycle.shtml.

[11] D. Bilitza *et al.*, J. Adv. Space. Res. **42**, 599 (2007).

[12] I. Langmuir *et al.*, Phys. Rev. **28**, 727 (1926).

[13] L. H. Brace, Geophysical Monograph **102**, 23 (1998).

[14] D. Thompson, *Tech. Rep.* SDL/03-300 Rev. C (Utah State University Space Dynamics Laboratory, Logan, 2003).

[15] S. Bauer *et al.*, Proc. of the IEEE **63**, 230 (1975).

[16] A. Barjatya, *Langmuir Probe Measurements in the Ionosphere* (Utah State University, Logan, 2007).